Universidad de La Laguna

Master's degree in Astrophysics
Universidad de La Laguna

Effect of central galaxy AGN activity on satellite galaxies in groups and cluster

Master's thesis

Student: Cruz Guerra, F. J.

Supervisor: Dalla Vecchia, C. & Negri, A.

July 2, 2018

Contents

Resumen

Uno de los objetos más interesantes y misteriosos del universo son los agujeros negros. Residen en el centro de la mayoría de las galaxias, regulando su crecimiento. La fuerza de atracción es tal que la materia es intensamente atraída y devorada. Cuando el ritmo de acrección sea máximo, el agujero negro emitirá a una luminosidad cercana al límite de Eddington. Por consiguiente, solo una pequeña parte de la materia acretada es devuelta hacia el medio exterior mediante chorros de partículas, colisionando con el gas del entorno y originándose un frente de choque. Esta radiación puede activar o detener la tasa de formación estelar tanto en la galaxia anfitriona como en el ambiente donde se propaga el choque. A su vez, estos vientos pueden afectar a la morfología de las galaxias que habitan en los grupos y cúmulos. Puede ser una de las claves para entender por qué cuanto más nos adentramos al centro de estas agrupaciones se hallan galaxias cada vez más rojas, con estrellas viejas y gas caliente (conocidas como elípticas y lenticulares), mientras que a distancias lejanas, sucede el caso opuesto (se observan galaxias espirales), de acuerdo con las observaciones. Asumiendo que el frente de choque se propaga a través del medio intracumular y se encuentra con otra galaxia en la misma dirección que viaja, si su presión vence a la gravitatoria de la misma expulsará su gas. Este proceso es conocido como ram-pressure stripping y depende de la distancia a la que se encuentren ambos. Además, este fenómeno también puede ocurrir mediante la interacción del gas intracumular con la galaxia (conocidas como "galaxias medusa", véase Figura 3). Otro mecanismo de sustracción del gas es la fuerza de marea entre dos galaxias.

Este proyecto está inspirado en el artículo de Nayakshin and Wilkinson (2013), en el cual estudiaron el efecto de stripping en galaxias enanas causado por una de dimensión comparable a la Vía Láctea. A su vez, dieron a entender que cuando el agujero negro que habita en la galaxia anfitriona está en su máxima actividad o crecimiento es capaz de parar la tasa de formación estelar de las galaxias satélites. En su trabajo, las galaxias satélite estaban formadas por un halo de materia oscura, gas bariónico y un disco de gas. Los autores presentaron tres modelos de choque, cuyo frente se propaga a velocidad constante de 300, 500 y 1000 km s^{-1}. Cuando la presión ejercida por el choque vence a la fuerza gravitatoria de la galaxia satélite, expulsa tanto el gas ubicado en el halo como en el disco. Mientras que el gas en el halo es prácticamente perdido a distancias bastante lejanas respecto al centro de la anfitriona, el disco mantendrá el gas a mayores trayectos, debido a que es más compacto y, por tanto, su fuerza gravitatoria resiste durante más tiempo la presión del frente de choque. El estudio lo llevaron a cabo para tres galaxias enanas a diferentes masas viriales, correspondientes a velocidades máximas circulares de 15, 30 y 60 km s^{-1} demostrando que la más masiva (60 km s^{-1}) conserva el gas durante un recorrido más largo respecto a la menos masiva (15 km s^{-1}), para ambos casos (halo y disco). Los experimentos se llevaron a cabo en el universo local.

En primer lugar, en §4.1.1 se analiza la fuerza gravitacional de la galaxia satélite como una función de la altura y del radio proyectado. La altura es fijada donde la aceleración total es máxima para todos los radios. Se observa que el bulbo es dominante únicamente a alturas y radios bastante cercanos al plano del disco, mientras que el disco estelar domina a alturas próximas al plano y radios donde el bulbo no destaca. El halo de materia oscura jugará un papel importante a alturas más alejadas de dicho plano y a radios cercanos al virial de la galaxia. Además, se demuestra que el efecto neto de todas las componentes es ligeramente superior a la presión gravitatoria propuesta por Gunn and Gott (1972), en el cual solo tuvieron en cuenta la presencia de disco estelar y de gas en la misma. Por último, se razona que esta presión es cada vez mayor a redshift altos, donde varía hasta un orden de magnitud entre cada z.

Este trabajo sigue en parte el procedimiento que llevaron a cabo Nayakshin and Wilkinson

(2013). A diferencia de su modelo, las galaxias satélites tienen además un disco estelar y un bulbo, lo que conlleva a fuerzas restauradoras más potentes. En §4.1.2 se reproducen las gráficas obtenidas por Nayakshin and Wilkinson (2013) usando sus parámetros y omitiendo el bulbo y el disco estelar únicamente en esta sección. Se focaliza solo en el modelo de frente de choque más energético, conocido como "NFW shell shock". Los resultados obtenidos para el disco de gas son idénticos, mientras que difieren para el halo cuya física sigue teniendo sentido, es decir, los halos más masivos conservan el gas en trayectos más largos. Por lo tanto, se confirma que el modelo puede ser aplicado a grandes escalas.

Seguidamente, en §4.2 se profundiza en el efecto de la presión del choque para diferentes ángulos de inclinación (0°, 30° y 60°) y velocidades del choque (1000, 1500 y 2000 km s^{-1}). El estudio se lleva a cabo desde bajo ($z = 0$), intermedio ($z = 1$) a alto redshift ($z = 2$). En concreto, se focaliza en altos valores de z ya que los discos van a ser más densos y pequeños respecto al universo local, siendo por tanto más difícil perder el gas. Además, esta situación también ocurre para el halo, pero su análisis carece de interés ya que prácticamente lo pierde todo a posiciones bastante lejanas del centro del cúmulo. Por otro lado, el halo que produce el frente de choque es del tamaño de grupos ($5 \times 10^{13}\ M_\odot$) y cúmulos de galaxias ($3 \times 10^{14},\ 2 \times 10^{15}\ M_\odot$), mientras que la masas de las satélites están comprendidas desde dimensiones comparables a la Vía Láctea ($\sim 10^{12}\ M_\odot$) a dos órdenes de magnitud menores ($10^{10}\ M_\odot$) de la misma. Se obtiene que para ángulos cada vez más grandes y para velocidades y masas del halo anfitrión más pequeñas, la presión del choque es más débil y, por tanto, la galaxia conserva el gas durante más tiempo. Además, se muestra que cuanto más masiva sea la satélite y el redshift es más alto, el efecto de stripping es menos efectivo, ya que la fuerza gravitatoria resiste a distancias más cercanas del centro del cúmulo.

Finalmente, se confirma que los resultados concuerdan con las observaciones y con otros modelos propuestos, por lo que la física aplicada es válida. Estos cálculos pueden ser verificados por comparación con simulaciones cosmológicas tales como EAGLE (Evolution and Assembly of GaLaxies and their Environments) y Cluster-EAGLE, los cuales investigan la formación y evolución de galaxias. En futuros proyectos se podría comprobar la contribución relativa de los choques a la ram-pressure stripping producida por el medio intracumular. Probablemente, la mayoría del gas ya habría sido removido por el efecto antes que la galaxia alcance distancias lo suficientemente pequeñas como para que los choques tengan un efecto apreciable.

1 Project objectives

Super-massive black holes (SMBHs) in central cluster galaxies drive strong outflows and shocks through the intra-cluster medium (ICM) during their maximum activity. We would like to know if these outflows and shocks can affect other galaxies in the cluster (reducing their star formation rate and their gas content through ram-pressure stripping, changing their colour, etc.). Specifically, this project focuses on the ram-pressure stripping process produced by shocks in the ICM generated by peaks of AGN activity. The project has been inspired by the work of Nayakshin and Wilkinson (2013). They hinted in the direction of a net effect in quenching star formation of satellite galaxies at the time of maximum AGN activity or SMBH growth. While they studied the effect of galactic winds of Milky Way-size galaxy starbusts on satellite, dwarf galaxies composed by a dark matter halo, baryonic gas and gas disc, this work partially follows their analytic model to be implemented on a large scales. Our model proposed defines the matter components of the satellite galaxy and group/cluster halo. On the contrary with their work, the satellite galaxy is also formed by stellar bulge and stellar disc. The former is expected to play a major role in the gravitational force for small radii and shorter height. The group or cluster one are constituted of a dark matter halo with intergalactic gas in the intra-cluster medium, the SMBH, which causes the outflow is placed in the centre of his halo. The stripping process is investigated for different satellite galaxies in haloes of masses, from 10^{10} to 10^{12} $M_{\odot}$ (Milky way-size). Consequently, the stripping radius is calculated numerically in order to determine the gas mass remained after a shock passage for different parameters: host halo virial mass, shock velocity and the inclination angle. The gas disc mass component is expected, proportionally, to retain more gas than the halo due to its higher surface density. This work explores the ram-pressure at low ($0 \leq z < 1$), intermediate ($1 < z < 2$) and high redshift ($z \geq 2$) by modelling an increasing the fraction of gas disc mass to stellar disc mass from 10% to 50%.

This project is structured as follows:

1. A brief theoretical development of black holes, AGN and ram-pressure stripping mechanism is described in §2. It has been also included a compilation of previous works.
2. The methodology used to undertake the quantitative study is explained in §3:
   - Numerical calculation of the stripping radius and the fraction of the mass retained of the satellite after the shock passage §3.1
   - Description of the dark matter halo (for host and satellite) in §3.2.
   - Depiction of the stellar and gas discs and stellar bulge of the galaxy (§3.3).
   - Procedure and parameters in order to obtain the main outcomes (§3.4).
3. Analysis of the results §4.
   - Study of the gravitational restoring force of the satellite galaxy (§4.1.1).
   - Testing the model against (Nayakshin and Wilkinson 2013)'s work in §4.1.2.
   - Applying the method to group and cluster size (§4.2).
4. A brief overview of the work, possible improvements of the model and future works in §5.

2 Introduction

Galaxy clusters and groups are the largest virialized structures in the Universe. They are systems gravitationally bound, containing from few tens to thousands galaxies and with virial mass $> 10^{14}$ $M_\odot$ ($> 10^{13}$ $M_\odot$ for groups) within a virial radius of ~ 1 Mpc. These clusters are composed mostly of dark matter, intergalactic gas in the intra-cluster medium (ICM) and galaxies. The baryonic mass is basically composed by fully ionized hydrogen and helium, with mean molecular weight $\mu \simeq 0.59$[1]. As the gas temperature is of the order of 10 million K, the ICM emits in X-rays.

Two of the most fascinating and interesting objects in the universe are **supernovæ (SNe)** and **Active Galactic Nuclei (AGN)**. The former occurs either in the last stage of a star's life, when the collapse overcomes the gravitational force or in a binary star system, when one of them is a white-dwarf that explodes due to saturation of accretion (Langer 2012). AGNs are the luminous centres of galaxies that have an active **Supermasive Black Hole (SMBH)**. In both cases, there is a massive object accreting inflowing matter (most of it is cold gas that converts its mechanical energy into thermal); an accretion disc will be formed due to the conservation of angular momentum. Due to the gas viscosity in the innermost parts of accretion disc, a relevant amount of energy is emitted in the form of direct radiation pressure or dense and powerful winds at very high speeds, known as **matter outflows and jets**. The cycle of gas inflow and outflow between intergalactic medium and galaxies is known as **feedback**[2] and plays an important role in regulating the growth of galaxies (Fabian 2012).

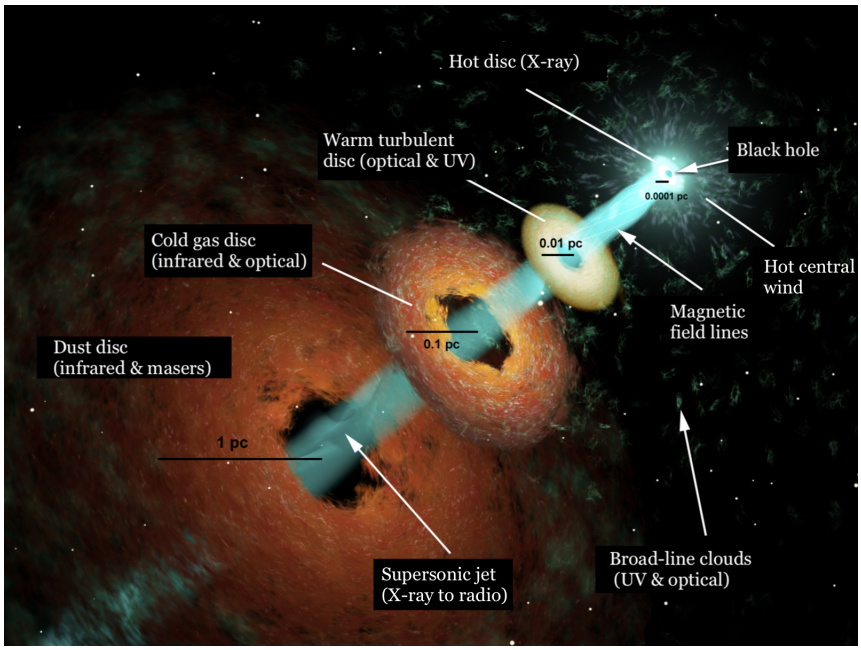

Figure 1: Impression of the inner structure of an Active Galaxy. Credit: (Gómez−Fernández and Steffen 2009).

A shock front is produced by the interaction between the outflow and the neighbouring gas in the intra-cluster medium (ICM) as depicted in Figure 2(a). The jets are dissipating energy until

[1]It has been calculated by $\mu = \frac{1}{2X+3/4Y+1/2Z} \simeq 0.59$, where $X \simeq 0.75$, $Y \simeq 0.23$ and $Z \simeq 0.02$ are the mass fraction in hydrogen, helium and metals, respectively.

[2]The observational evidence for AGN feedback is found in several galactic outflows. The term *blazar* is viewing down the jet and *quasar* viewing at an angle to the jet.

stopping in a hot spot, where a backflow is produced. These powerful winds inflate **bubbles** or **radio lobes**, filled with relativistic hot plasma which emits synchrotron radiation. The radiation is detected at radio frecuencies, and radio lobes are also visible as surface brightness depressions, or **cavities**, in X-ray imaging[3]. The cocoons will expand, driving a shock wave (Boettcher, Harris, and Krawczynski 2012).

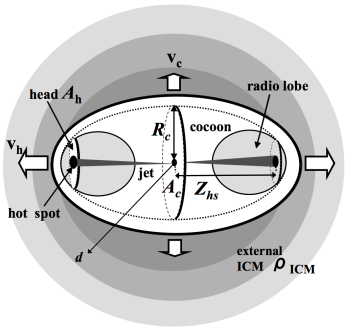

(a) A schematic representation of the shock. The region between the cocoon and the external ICM is called as shock shell. Credit: (Kino et al. 2009).

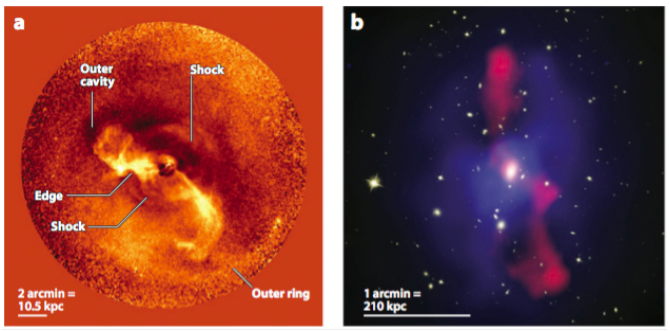

(b) The most energetic outburst actually have been seen in cluster MS0735.6. one can determine how much energy is produced by the black hole by measuring how much gas is moved. Left: The Arms and weak shocks produced by the jets of M87. Credit: (Forman et al. 2007). Right: The gigantic interaction of the radio lobes and intracluster gas of MS0735.6, seen in X-ray, visible and radio wavelength. Credit: (McNamara et al. 2009).

Figure 2: Both figures illustrate how is the interaction between the outflow and the neighbouring gas in the intra-cluster medium (ICM).

On the other hand, under the assumption that an object is spherical in shape with mass M and radius R, the energy output per unit of time known as **luminosity** L, depends on how mass accretes per unit of time, accretion rate $\dot{M}$:

$$L = \frac{\Delta E}{\Delta t} = \frac{GM\dot{M}}{R} \tag{1}$$

where G is the gravitational constant. The luminosity that counterbalances, through the repulsive radiation effect of radiation, the gravitational force driving the inflow, is known as the **Eddington limit**, in other words, the maximum luminosity that an object can emit. If the inflowing matter is pure hydrogen completely ionized, the maximum luminosity is given by

$$L_{\mathrm{Ed}} = \frac{4\pi cGMm_{\mathrm{p}}}{\sigma_{\mathrm{T}}} \simeq 1.3 \cdot 10^{38} \frac{M}{M_{\odot}} \text{ erg s}^{-1} \tag{2}$$

where c the speed of light, m_{p} the mass of the proton and σ_{T} the Thomson cross section. The previous equation only depends on the mass of the object. The hypothesis is established that the object is a black hole with mass M_{BH} emits at maximum luminosity during a time t_{BH}[4] which is really short in comparison with the dynamic time of a cluster. Furthermore, it is supposed that only a small fraction of this energy interacts with the gas of the external environment, α_{BH}. Therefore, the total amount of energy deposited in that period can be obtained through

[3]This cavities have lower density than their surroundings. It is a result of the interaction between the ICM and the jet. The shock shell is denser.

[4]It is also known as duty cycle.

Equation 1

$$E_{\rm BH} \simeq \kappa M_{\rm BH} \alpha_{\rm BH}\ t_{\rm BH} \tag{3}$$

with κ is a constant factor.

According to Fabian (2012), AGN feedback is found in observations in two accretion modes: **kinetic (jet, radio) mode** and **radiative (wind, quasar) mode**[5]. The former occurs when the black hole accretes at a low Eddington ratio and corresponds to massive galaxies with low-luminosity AGNs ($L_{\rm BH} < L_{\rm Ed}/100$), observed at low redshift. The latter takes place when the black hole accretes close to the Eddington limit, where the AGNs are very luminous, driving high-velocity outflows $v_{\rm AGN} \sim 0.1\ c$ at high redshift (King 2003).

There is a link between feedback from AGN and supernovæ and the **Star Formation Rates (SFRs)** of the host galaxy (Benson 2010). In addition, feedback can be either positive or negative. The outflow compresses the gas enhancing cooling (as cooling is a function of the gas density ρ^2 (Cattaneo et al. 2009)). On the other hand, jets can heat and disperse the gas in the interstellar medium (ISM), reducing the star formation. Moreover, the AGN negative feedback can explain the lack of cold gas in dense cluster cores as is seen in observations, known as **cooling-flow** problem (Domainko et al. 2004).

AGN jets are notably important because they might explain the **transformation of galaxy morphology** in cluster/groups of galaxies and high-density environments. There is a relation between the composition of the galaxy and the clustercentric radius: earlier-type (ellipticals and lenticulars) galaxies, the most massive galaxies in the Universe, are redder, older and more luminous than galaxies farther from the cluster centre, later-type (spirals) (Diaferio et al. 2001). von der Linden et al. (2010) showed that star formation has been suspended almost 80% in the cluster centre and spiral galaxies has an abundant of cold gas facilitating the existence of stars.

One mechanism that could strip gas out of galaxies. One of them is **tidal stripping**, that occurs when a galaxy overcomes the gravitational force and expels the gas and stars from a neighboring smaller galaxy (Patterson and Thuan 1992). This project aims at studying the **ram-pressure stripping mechanism (RPS)**: in clusters, it is mostly given by galaxies orbiting in the ICM which experience an encounter with it and shocks as has been explained above. As a consequence, the gas in the galaxy is stripped. Galaxies which have suffered this effect are so-called **jellyfish galaxies** whose "tentacles" are the lost gas in the process. This phenomenon can be seen in Figure 3, whose pictures have been taken from GASP (GAs Stripping Phenomena in galaxies with MUSE15 spectrograph) program that study this process. Poggianti et al. (2016) proposed some jellyfish galaxy candidates in galaxy clusters at low redshift.

[5]The usualest way in which AGN winds are detected by line absorption of the quasar continuum by acting wind material (the UV spectrum can be directly observed).

(a) ESO 137-001: A spiral galaxy in the Norma cluster over 200 million light years from Earth. Credit: X-ray: NASA/CXC/UAH/M.Sun et al, blue color; Optical: NASA, ESA, the Hubble Heritage Team (STScI/AURA), cyan, orange and white colors.

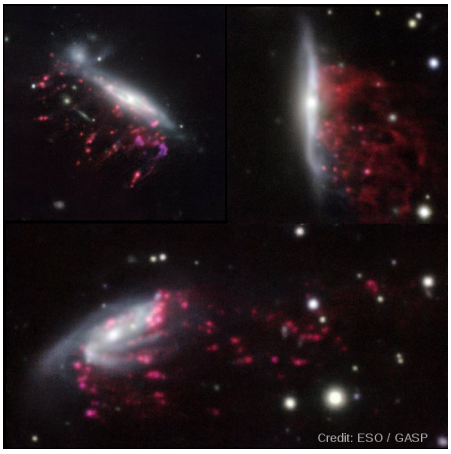

(b) Upper left: JO204. Lower left: JW206. Upper right: JW100. Credit: (collaboration 2017a), (collaboration 2017c) and (collaboration 2017b), respectively.

Figure 3: Examples of jellyfish galaxies.

Let us imagine a satellite galaxy within a gaseous intracluster medium of density $\rho_{\rm ICM}$ that is moving at a relative velocity $v_{\rm ICM}$. If the ram pressure $P_{\rm ram}$ leads to the gravitational restoring force per unit of area of the galaxy $P_{\rm grav}$ in the direction to the line of sight (vertical dashed line), for a face-on encounter, the gas in the satellite will be stripped. The transition radius at which both pressures counterbalance one another is denominated **stripping radius** $R_{\rm st}$ (if $R > R_{\rm st}$ all gas inside the satellite galaxy is lost):

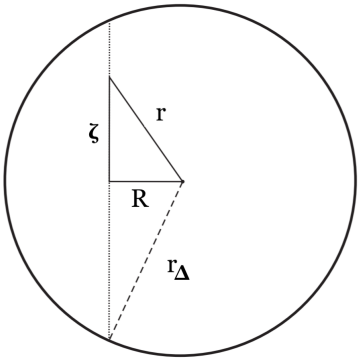

Figure 4: A schematic diagram of the spherical dark matter halo seen in cylindrical coordinates. The stripping process takes place in the direction of line of sight. R is projected distance in the plane of the sky and ζ the height.

$$P_{\rm ram} = P_{\rm grav}(R_{\rm str}, \zeta) \;\rightarrow\; \rho_{\rm ICM} v_{\rm ICM}^2 = \Sigma_{\rm gas}(R_{\rm str}) \frac{\partial \phi}{\partial \zeta}(R_{\rm str}, \zeta) \tag{4}$$

where $\Sigma_{\rm gas}(R_{\rm str})$ the gas surface density and $\frac{\partial \phi}{\partial \zeta}(R, \zeta)$ the acceleration of each component that form the galaxy. It would be preferable to work in cylindrical coordinates, as the stripping process occurs in the direction of line of sight. The gravitational acceleration $\frac{\partial \phi}{\partial z}(R, \zeta)$ depends on the height ζ at a given projected distance in the plane of the sky, R. In addition, any height

is not possible to consider because this gradient is zero in the disc plane ($\zeta = 0$). This problem will be discussed later.

The original work in order to investigate the RPS was carried out by Gunn and Gott (1972) which proposed a simple case of expelling the gas from the interstellar medium (ISM) in spiral galaxies. They just took account the gravitational acceleration from the stellar disc $\frac{\partial \phi_*}{\partial z}(R, \zeta)$ which is associated with its surface density $\Sigma_{\rm d}(R)$ as

$$\frac{\partial \phi_*}{\partial \zeta}(R_{\rm str}) = 2\pi G \Sigma_*(R_{\rm str}) \tag{5}$$

Hence, Equation (4) can be rewritten as

$$P_{\rm ram} = P_{\rm grav}(R_{\rm str}) \quad \rightarrow \quad \rho_{\rm ICM} v^2_{\rm ICM} = 2\pi G \Sigma_*(R_{\rm st}) \Sigma_{\rm d}(R_{\rm st}) \tag{6}$$

where $\Sigma_{\rm d}(R)$ is the gas disc surface density. In this case, $R_{\rm str}$ can be easily obtained analytically. Some years later, several works investigated the stripping process for different satellite galaxies and outflows/winds: while supernova-driven winds can expel the intergalactic gas out in dwarf galaxies within groups and clusters (Dekel and Silk 1986); the pressure exerted by supernova winds is not efficient to overcome the gravitational force from more massive galaxies. Then, AGN outflows will be more effective in order to drive the gas out in high-mass galaxies. In the past decades, Researchers have used hydrodynamical simulations in order to investigate this mechanism as well: Murakami and Babul (1999) focused on effect of the external medium on evolution of supernova-driven outflows from dwarf galaxies; Abadi, Moore, and Bower (1999) proposed a more realistic spiral galaxy model in order to describe the Milky Way, with bulge and dark matter halo following the profiles described by Hernquist (1993). In contrast to Gunn and Gott (1972) work, their galaxy was formed with more components, so their corresponding contribution to the gravitational restoring force were taken into account. In this paper, the authors showed that for small radii the bulge just plays an important role in gravitational restoring force of galaxy, being negligible at larger radii where the halo starts dominating. The authors mentioned above studied the RPS for different inclination angles for the wind, showing that inclined disc galaxies (edge on respect to the wind) orbiting in clusters remain the double of gas than a face on encounter. Moreover, the stripping process in a face on view takes place in radii closed to Gunn and Gott (1972) criterion. On the other hand, Marcolini, Brighenti, and D'Ercole (2003) investigated the ram pressure stripping in dwarf galaxies where outflows are coming from groups of galaxies. They analyzed this process as a function of different parameters such as galactic mass and velocity, ambient gas density and the inclination angle between galactic plane and orbital plane. Mayer et al. (2006) showed that tidal stripping is less efficient to drive the gas out from spheroidal galaxies (dSphs) going around a host galaxy such as Milky Way than the tidal and ram pressure stripping together. Roediger and Brüggen (2007) focused on the retained gas mass of a galaxy orbiting in a cluster varying the inclination angle. Their results are similar to the Gunn and Gott (1972) criterion for stripping process not closed to edge-on encounter, provided that the ram pressure does not rise the characteristic stripping time in which case the amount of retained gas disc is slightly greater than expected.

Nayakshin and Wilkinson (2013) showed that the gas in the satellite dwarf galaxies orbiting the parent is affected by the RP of galactic outflows driven by either quasars/AGNs or powerful starbursts coming from the host. They hinted in the direction of a net effect in quenching star formation in satellites at the time of maximum AGN activity or SMBH growth. Their analytic model consisted of a **host halo** whose dark matter distribution follows the profile proposed by Navarro, Frenk, and White (1997) with baryonic gas and a **satellite galaxy** that orbits at a distance $\Re$ from the center of the parent one. The latter is also formed by a halo and a gas disc

based on Mo, Mao, and White (1998) work. They proposed three different ways to describe the ram pressure. In the most energetic one, known as **NFW shell**, the satellite suffers an encounter with a moving shell with a constant velocity $V_{\rm sh}$. The shell's mass, fixed fraction $f_{\rm sh}$ of the total mass enclosed in the host's halo $M_{\rm enc}(< \Re)$ (baryonic and dark matter at a given galactocentric $\Re$ distance), increases as it travels outward

$$M_{\rm sh}(< \Re) = f_{\rm sh} M_{\rm enc}(< \Re) \tag{7}$$

During the stripping process, the outflow coming from the AGN activity collides with the environment, producing a shock front moving at a constant velocity $V_{\rm sh}$ with gaseous shell of density $\rho_{\rm sh}(\Re)$, given by

$$\rho_{\rm sh}(\Re) = \frac{M_{\rm sh}(< \Re)}{4\pi \Re^2 \Delta \Re} \tag{8}$$

where $\Delta\Re < \Re$ is the radial thickness of the incoming shell and $M_{\rm sh}(< \Re)$ the mass of the shell. This shock front is the responsible for the transformation of the satellite galaxy. Consequently, the shock can remove gas from the galaxy depending on the distance $\Re$. Where the instantaneous ram pressure $\rho_{\rm sh}(\Re)V_{\rm sh}^2$ exceeds the local gravitational restoring force per unit of area from the satellite galaxy, the gas is stripped. As they considered independently the ram pressure effects on both these gas components, they determined the stripping radius $R_{\rm st}$ for the case of the gas disc and another for the gas halo. Then, the authors calculated the fraction of gas mass that is retained by the satellite galaxy $\delta_{\rm ret}(< \Re)$, integrating the gas mass profile up to the stripping radius normalized to the total; original gas mass within the virial radius.

Finally, Nayakshin and Wilkinson compared the energy that emits a black hole at its maximum activity using the equation from (King 2003) to the total kinetic energy from the outflow of the NFW shell model, given by

$$E_{\rm sh} = \frac{1}{2} M_{\rm sh_T} V_{\rm sh}^2 \tag{9}$$

where $M_{\rm sh_T}$ is the total mass of the shell driven outward to the virial radius of the host galaxy.

The idea of this project is to see if the shock contribution to ram-pressure stripping caused by cluster-size shocks is substantial in satellite galaxies from 10^{10} $M_\odot$ to Milky Way-size. (Nayakshin and Wilkinson 2013) work is followed, introducing more components in the satellite and studying the effect for different inclination angles as in Roediger and Brüggen (2006). This project is conducted from low ($0 \leq z < 1$), intermediate ($1 < z < 2$) to high redshift ($z = 2$). The higher the redshift the more compact the galaxy, confirmed by observations (Bezanson et al. 2009; Trujillo et al. 2007; van Dokkum et al. 2010); it is expected that discs are smaller and denser with higher surface densities e.g. (Dutton et al. 2011). As a consequence, similar spiral galaxies at high redshift will retain more gas than galaxies of similar mass at low redshift because their gravitational restoring force is stronger.

3 Methodology

The methodology followed in the project is explained here. The analytic model consists of:

- A **host halo** whose dark matter distribution follows the (Navarro, Frenk, and White 1997)'s model.
- A **satellite galaxy** formed by a dark matter halo with baryonic gas, a stellar disc, a gas disc and a stellar bulge located at its center.

In §3.1 starts explaining how the stripping process is carried out and how the stripping radius is numerically obtained. Considering that the gas is distributed both in the halo and in the disc, this radius is independently calculated. Then, the fraction of the mass retained after the shock passage is defined here.

The dark matter distribution in groups/clusters and satellites are based on (Navarro, Frenk, and White 1997) (§3.2). Likewise, the gas halo surface density and the gravitational acceleration are defined in order to obtain the contribution to the gravitational restoring force of the satellite. Finally, the fraction of the gas halo mass retained by the gas component is calculated, integrating up to the radius of stripping for that particular case.

Once the halo is defined, the gravitational force exerted by the discs and the stellar bulge are obtained in §3.3. In addition, it is also mentioned how much mass the gas disc holds during the RPS process.

Lastly, the procedure to determine the results is described in §3.4

3.1 Modelling ram pressure stripping effects

All galaxy components in the gravitational restoring acceleration are deemed (denoted as stellar ($*$) and gas disc (d), stellar bulge (b), dark matter halo (NFW) and baryonic gas halo (NFW_g)) and the projection cosine law is included with the aim to study the ram pressure for different angles Ψ between the outflow direction and the disc plane of the satellite, as in Roediger and Brüggen (2006). As the gas distribution in the halo and in the gas disc is assumed individually, their respective stripping radius can be independently obtained (R_{str_h} and R_{str_d}, respectively). The performance of the ram pressure stripping is different for each galaxy component, the gas contained in the halo is expected to be stripped easier than gas in the disc because it is less compact, thus the gravitational restoring force is lower. It should be noted that the temporal variation of the ram pressure process is neglected. In other words, the process is instantaneous and only depends on the distance between the satellite and host galaxy $\Re$. In addition, tidal stripping process is not considered because in the project is assumed that satellite galaxies have not yet had time to interact with other galaxies on the central galaxy. Using Equation 4 and taking into account all satellite galaxy components, one can solve numerically for calculating the stripping radius $R_{\text{str}_{\text{d,h}}}$[6]

$$\begin{aligned}\rho_{\text{sh}}(\Re)V_{\text{sh}}^2\cos(\Psi) = \\ = \Sigma_{\text{gas}}(R_{\text{str}_{\text{d,h}}})\Bigg(\frac{\partial\phi_*}{\partial\zeta}(R_{\text{str}_{\text{d,h}}},\zeta) + \frac{\partial\phi_{\text{d}}}{\partial\zeta}(R_{\text{str}_{\text{d,h}}},\zeta) + ... \\ ... + \frac{\partial\phi_{\text{b}}}{\partial\zeta}(R_{\text{str}_{\text{d,h}}},\zeta) + (1+f_h)\frac{\partial\phi_{\text{NFW}}}{\partial\zeta}(R_{\text{str}_{\text{d,h}}},\zeta)\Bigg)\end{aligned} \tag{10}$$

[6]The notation of d, and h means the equation are solved separately for the disc and halo case, respectively.

where $\Sigma_{\rm gas}(R)$ is the surface density of the gas at any radius ($\Sigma_{\rm d}(R)$ for the disc and $\Sigma_{\rm NFW,g}(R)$ for the halo). The gravitational acceleration $\frac{\partial\phi}{\partial\zeta}(R,\zeta)$ depends on the height ζ at a given stripping radius $R_{\rm str_{d,h}}$. Roediger and Hensler (2005) suggested the possibility to choose either the maximal restoring force inside the disc or the maximal at any height (see their Figures 8 and 9). They showed that both choices are quite similar, differing only at low ram pressures. The criterion in this model, which will be explain in detail in S§4.1.1, is to choose the gravitational acceleration maximum along the ζ-direction for any radii. In this way, the galaxy will resist further to the stripping

$$\begin{aligned}\rho_{\rm sh}(\Re)V_{\rm sh}^2\cos(\Psi) = \\ = \Sigma_{\rm gas}(R_{\rm str_{d,h}})\left(\frac{\partial\phi_*}{\partial\zeta}(R_{\rm str_{d,h}})\Big|_{\rm max} + \frac{\partial\phi_{\rm d}}{\partial\zeta}(R_{\rm str_{d,h}})\Big|_{\rm max} + ... \right. \\ \left. ... + \frac{\partial\phi_{\rm b}}{\partial\zeta}(R_{\rm str_{d,h}})\Big|_{\rm max} + (1+f_h)\,\frac{\partial\phi_{\rm NFW}}{\partial\zeta}(R_{\rm str_{d,h}})\Big|_{\rm max}\right)\end{aligned} \tag{11}$$

The previous expression can be solved by finding zeros for a given value of $\Re$ and Ψ. The corresponding surface density is applied

$$y_{\rm d,h}(\Re,\Psi,R_{\rm str_{d,h}}) = F_{\rm grav}(R_{\rm str_{d,h}})\Big|_{\rm max} - F_{\rm ram}(\Re,\Psi) = 0 \tag{12}$$

Hence, three possibilities are found:

1. $\boldsymbol{y_{\rm d,h}(\Re,\Psi,R_{\rm str})\Big|_{\rm min} > 0}$: The gravitational force exerted by the galaxy dominates and the function is positive for any radius. As a result, it keeps its gas at all times, so the stripping radius is set at which
   - the radius of the gas disc $R_{\rm str_d} = R_{\rm max_d}$ (gas disc case)
   - the virial radius of the satellite galaxy $R_{\rm str_h} = R_\Delta^{\rm sat}$ (gas halo case).
2. If $\boldsymbol{y_{\rm d,h}(\Re,\Psi,R_{\rm str})\Big|_{\rm max} < 0}$: The ram pressure always overcomes the gravitational one, so the function $y_{\rm d,h}$ is negative for all radii. As a consequence, the gas is lost in any time, so $R_{\rm str_{d,h}} = 0$.
3. **Otherwise**: both forces are dominant at a certain point. The function $R_{\rm str_{d,h}}(y_{\rm d,h}=0)$ is interpolated in order to find the zero.

In order to study what fraction of gas mass is retained by the satellite galaxy $\delta_{\rm ret_{d,h}}(<R_{\rm str_{d,h}})$, the gas mass profile is integrated up to the stripping radius $M_{\rm g}(<R_{\rm str_{d,h}})$ normalized to the total; original gas mass within the virial radius $M_{\rm g}(<R_\Delta)$. Only the gas within the satellite galaxy can be removed because dark matter particles and stars[7] are not affected by the interaction between shock front and galaxy. Then, the fraction of the retained mass is calculated numerically using the Trapezoidal Rule Technique.

$$\delta_{\rm ret}(R_{\rm st}) = \frac{M_{\rm g}(<R_{\rm st})}{M_{\rm g}(<R_\Delta)} \tag{13}$$

[7] However, in reality, stars can be moved.

3.2 Dark matter halo

The standard model that describes the formation of the structure in the Universe and can explain the cosmological observations is the **Lambda Cold Dark Matter model (ΛCDM)**. It is defined by Cold Dark Matter (CDM) and dark energy, described by the cosmological constant Λ, which produces the acceleration in the expansion of the universe. From Einstein's formulæ for the gravitational field in the Robertson-Walker metric (homogeneous and isotropic case) (Robertson 1935), (Robertson 1936a), (Robertson 1936b) and (Walker 1935), Friedmann differential equation is used in order to determine the normalized rate of the expansion, the **Hubble parameter** $H(z)$ at a given redshift z. The solution to the Friedmann eq. in a flat universe[8] is

$$H(z) = H_0\sqrt{\Omega_{\mathrm{M},0}(1+z)^3 + \Omega_\lambda} \tag{14}$$

where H_0 is the Hubble constant at present time, $\Omega_{\mathrm{M},0}$ is the present day matter density parameter (dark and baryonic) and the constant cosmological density parameter is such that $\Omega_{\mathrm{M},0} + \Omega_\lambda = 1$. The **critical density of the universe** $\rho_{\mathrm{crit}}(z)$ is given by

$$\rho_{\mathrm{crit}}(z) = \frac{3H^2(z)}{8\pi G} \tag{15}$$

The Spherical Top-Hat model was first introduced by Gunn and Gott (1972), that is about a spherical perturbation of uniform overdensity in the Universe. When the sphere reaches the virial equilibrium with mass M and radius R enclosing a given density contrast Δ_c above the ρ_{crit} (last stage of the collapse) is known as a **halo**. The halo will be formed by dark and baryonic matter. The evolution of the halo overdensity with redshift is

$$\Delta_c = 18\pi^2 + 82\chi - 39\chi^2 \tag{16}$$

with $\chi = \Omega(z) - 1$ and $\Omega(z) = \Omega_{\mathrm{M},0}(1+z)^3\left[H(z)/H_0\right]^{-2}$ (Bryan and Norman 1998). The halo's average density is given by

$$\rho(< r_\Delta) = \Delta_{\mathrm{c}}(z)\rho_{\mathrm{crit}}(z) = \frac{M(< r_\Delta)}{\frac{4}{3}\pi r_\Delta^3(z)} \tag{17}$$

where $M(< r_\Delta)$ is the total mass within **virial radius** $r_\Delta(z)$, defined as the radius at which the halo density is Δ_c times the critical density at a given redshift. Inserting eq. 15 in eq. 17, its expression is estimated as follows

$$r_\Delta(z) = \left(\frac{2M_\Delta G}{\Delta_{\mathrm{c}}(z)H^2(z)}\right)^{1/3} \tag{18}$$

where the virial mass is the mass within the virial radius $M_\Delta \equiv M(< r_\Delta)$ (the sum of dark and baryonic masses). The circular velocity at the virial radius of the dark matter halo is given by (Mo, Mao, and White 1998)

$$V_\Delta = \sqrt{\frac{GM_\Delta}{r_\Delta}} = 10H(z)r_\Delta \tag{19}$$

On the other hand, Navarro, Frenk, and White (1997) described the dark matter density profile of haloes in equilibrium with a universal empirical law analyzing high-resolution N-body simulations for different cosmologies. This is well-fitted by the following function

$$\rho_{\mathrm{NFW}}(r) = \rho_{\mathrm{crit}}(z)\frac{\delta_c}{(r/r_{\mathrm{s}})\left(1 + r/r_{\mathrm{s}}\right)^2} \tag{20}$$

[8] No curvature.

where $r_{\rm s}$ is the scale radius (radius at which the density profile changes slope), $c(z)$ the halo concentration parameter (ratio of virial radius to scale radius) $c(z) = r_\Delta(z)/r_{\rm s}$, and $\delta_{\rm c}(z)$ characteristic dimensionless density

$$\delta_c(z) = \frac{\Delta_c(z)}{3}\frac{c^3}{f(c)} \tag{21}$$

with $f(c) = \ln(1+c) - \frac{c}{(1+c)}$. In other to obtain the concentration parameter as a function of the virial mass and redshift, Eq. (5)-(7) has been used from (Muñoz-Cuartas et al. 2011). This density profile drops from a logarithmic slope -1 in the inner parts to -3 in outer parts. Rearranging Eq. 20 as Eq. D3 in (Wang et al. 2010), the halo's density distribution is now a function of the projected distance in the plane of the sky R and the height ζ

$$\rho_{\rm NFW}(R,\zeta) = \frac{M_\Delta}{4\pi f(c) r_\Delta}\frac{cx}{r^2(1+x)^2} \tag{22}$$

with $x = r\ /r_{\rm s}$ and $r = \sqrt{R^2+\zeta^2}$. The gas surface density in the halo is estimated by projecting the three dimensional halo density along the line of sight

$$\Sigma_{\rm NFW,g}(R) = 2f_{\rm h}\int_0^{\sqrt{\rm r_\Delta^2 - R^2}} dz\ \rho_{\rm NFW}(z) = 2f_{\rm h}\int_R^{\rm r_\Delta} dr\ r\frac{\rho_{\rm NFW}(r)}{\sqrt{r^2-R^2}} \tag{23}$$

The dark matter mass within a radius r is determined by

$$M_{\rm DM}(<r) = 4\pi\int_0^r dr'\ r'^2\rho_{\rm NFW}(r') = 4\pi\rho_{\rm crit}(z)\delta_{\rm c}r_{\rm s}^3\left[\ln\left(\left|1+\frac{r}{r_{\rm s}}\right|\right) - \frac{r}{r+r_{\rm s}}\right] \tag{24}$$

A simple assumption for the baryon mass in the halo is to consider it as a fixed fraction of $f_{\rm h}$ of the dark matter mass

$$M_h(<r) = f_{\rm h}M_{\rm DM}(<r) \tag{25}$$

On the other hand, once the halo's properties have been defined, the halo gravitational acceleration produced by the dark matter density is determined through Poisson's equation

$$\nabla^2\phi(r) = 4\pi G\rho(r) \tag{26}$$

The previous equation is broken down in cylindrical coordinates and is integrated along ζ direction, obtaining the force per unit of mass produced by the dark matter and the gas halo

$$\frac{\partial\phi_{\rm NFW}(R,\zeta)}{\partial\zeta} = -\frac{GM_\Delta}{f(c)}\left(\frac{c}{r_\Delta}\right)^2\frac{\frac{x}{(1+x)} - \ln(1+x)}{x^2}\frac{\zeta}{\sqrt{R^2+\zeta^2}}; \qquad \frac{\partial\phi_{\rm NFW,g}(R,\zeta)}{\partial\zeta} = f_h\frac{\partial\phi_{\rm NFW}(R,\zeta)}{\partial\zeta} \tag{27}$$

where $\phi_{\rm NFW}(R,\zeta)$, $\phi_{\rm NFW}(R,\zeta)$ are the dark matter and gas halo potentials, respectively.

Finally, the retained gas halo mass fraction for the satellite galaxy after the interaction with the shock front is obtained by the means of Equation 13

$$\delta_{\rm ret,h}(R_{\rm str_h}) = \frac{f_{\rm h}M_{\rm DM}(<R_{\rm str,h})}{f_{\rm h}M_{200}} = \frac{4\pi f_{\rm h}\int_0^{R_{\rm str_h}} dR'\ R'^2\rho_{\rm NFW}(R',\zeta_{\rm max})}{f_{\rm h}M_{200}} \tag{28}$$

3.3 Satellite galaxy

Different profiles have been used in order to define the components of the **satellite galaxy**. As it is mentioned before, the dark matter halo follows Navarro, Frenk, and White (1997) one, as in the case of the host. Both the stellar and gas dics are assumed to follow the models of Hernquist (1993) and Mo, Mao, and White (1998). Lastly, stellar bulge is based on (Hernquist 1993). As it is wanted to read up on the dependence on the ζ coordinate in the gravitational acceleration, the system is defined by cylindrical coordinates.

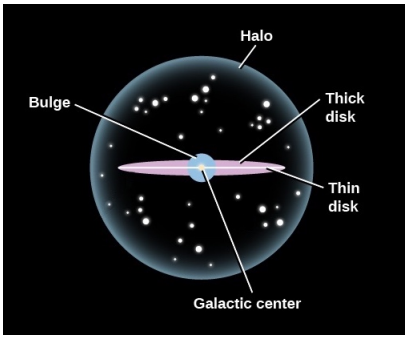

Figure 5: Satellite galaxy. Edge on view.

3.3.1 Stellar and gas disc

In addition to being composed by a dark matter halo, the satellite galaxy is also defined by a stellar and gas disc. The density profiles of both are expressed as in (Hernquist 1993)

$$\rho_{*,d}(R,\zeta) = \rho_{*0,d0}\exp\left(-R/R_{*,\mathrm{d}}\right)\,\mathrm{sech}^2(\zeta/\zeta_{*,\mathrm{d}}) \tag{29}$$

where $\rho_{*0,\mathrm{d}0} = \frac{M_{*,\mathrm{d}}}{4\pi R_{*,\mathrm{d}}^2 z_{*,\mathrm{d}}}$, $R_{*,d}$ is the scale length and $\zeta_{*,d}$ the scale height of the isothermal disc. Their respective surface densities profiles at radius R from the centre of the satellite galaxy, projected along the direction from the centre of the host, is determined by

$$\Sigma_{*,\mathrm{d}}(R) = 2\int_0^\infty d\zeta'\rho_{*,\mathrm{d}}(R,\zeta) = 2\zeta_{*,d}\;\rho_{*0,\mathrm{d}0}\exp\left(-R/R_{*,\mathrm{d}}\right) = \Sigma_{*,\mathrm{d}0}\exp\left(-R/R_{*,\mathrm{d}}\right) \tag{30}$$

respectively. The central surface density Σ_{*0}, as in (Mo, Mao, and White 1998), may be obtained through

$$\Sigma_{*0} = \frac{M_*}{2\pi R_*^2} = \frac{f_* M_\Delta}{2\pi R_*^2} = \frac{f_* V_\Delta^3}{20GH(z)\pi R_*^2} \tag{31}$$

Eq. 19 has been used in the previous formula. The total stellar disc mass M_* is supposed to be a fixed fraction of f_* of the halo mass, which was contained between $[0.05, 0.1]$ at redshift $z = 0$ (Mo, Mao, and White 1998). Moreover, the relationship between central surface density of the stellar and the gas disc is the same that the stellar mass and the gas mass, denoted by f_d. It is therefore possible to estimate the gas disc mass

$$\frac{\Sigma_{\mathrm{d}0}}{\Sigma_{*0}} = \frac{M_\mathrm{d}}{M_*} = f_\mathrm{d} \quad \rightarrow \quad M_\mathrm{d} = f_\mathrm{d} M_* \tag{32}$$

the fraction of gas disc mass to stellar disc mass $f_{\rm d}$ depends on the redshift (Geach et al. 2011)

$$f_{\rm d} \sim (1+z)^{2.0\pm0.5} \tag{33}$$

Once the density and all its parameters have been defined, in order to find the contribution of the stellar and gas disc to the gravitational restoring force, the gravitational acceleration generated by their mass distribution is obtained by solving Equation 26. The radial variation compared to the vertical one is neglected if the discs are assumed thin

$$\left|\frac{\partial}{\partial R}\left(R\frac{\partial\phi(R,\zeta)}{\partial R}\right)\right| << \left|\frac{\partial\phi(R,\zeta)^2}{\partial\zeta^2}\right| \tag{34}$$

Hence, integrating respect to the height ζ, the gradient of the potential is

$$\frac{\partial\phi_{*,\rm d}(R,\zeta)}{\partial\zeta} = 4\pi G\zeta_{*,\rm d}\frac{M_{*,\rm d}}{4\pi R_{*,\rm d}^2\zeta_{*,\rm d}}\exp\left(-R/R_{*,\rm d}\right)\tanh\left(\zeta/\zeta_{*,\rm d}\right) \tag{35}$$

Finally, using the stripping radius for the case of the disc (Eq. 12), the fraction of the mass retained for this case is defined by the means of Equation 13

$$\delta_{\rm ret,d}(R_{\rm str,d}) = \frac{M_{\rm d}(<R_{\rm str,d})}{M_{\rm d}} = \frac{2\pi\int_0^{R_{\rm str,d}} dR'\ R'\ \Sigma_{\rm d}(R')}{M_{\rm d}} \tag{36}$$

3.3.2 Bulge

Last component of the satellite is a spherical bulge, which has a volumetric density based on Henquist profile (Hernquist 1993):

$$\rho_{\rm b}(r) = \frac{M_{\rm b}}{2\pi r}\frac{R_{\rm b}}{(r+R_{\rm b})^3} \tag{37}$$

where its scale radius is R_b and its mass $M_{\rm b} = f_{\rm bulge}\ M_*$. Likewise, the bulge generates an isochrone potential, whose force per unit of mass is given by

$$\frac{\partial\phi_{\rm b}(R,\zeta)}{\partial z} = \frac{GM_{\rm b}}{(r+R_{\rm b})^2}\frac{\zeta}{r} \tag{38}$$

3.4 Procedure and parameters

Firstly, the assumptions in both models are shown in §3.4.1, while the differences are exposed in §3.4.2. Secondly, the gravitational force is studied in §4.1.1 using the values of Table 1 (§3.4.3). (Nayakshin and Wilkinson 2013)'s results are reproduced in §4.1.2, neglecting the contribution of the stellar bulge and disc with values given in Table 2. Finally, including the previous terms, the model is used in order to make a deep study of the stripping effect implemented on large scales (§4.2). Several parameters which has been considered appropriate are modified to observe their impact in the satellite. In addition, values of Table 1 are employed in §3.4.4 for different satellite and host masses, inclination angle and shock velocities.

3.4.1 Common assumptions

Common assumptions that are made throughout the project are the following

- In agreement with the majority of papers which proposed values for haloes overdensities at 200, the variation respect to redshift is neglected. It is set to be $\Delta_{\rm c}(z) \equiv 200$.
- The stellar and disc scale length for the satellite galaxy are equals, set up to $R_{*,\rm d} = 0.05\ R_{200}^{\rm sat}$ as in §3 (Nayakshin and Wilkinson 2013).
- The fraction of the mass of the shell to the total mass enclosed in the host' halo is set to be $f_{\rm sh} = 0.05$.
- Both scale height are supposed to be equals and set to $z_{*,\rm d} \sim 0.06\ R_{*,\rm d}$.
- The radial thickness of the incoming shell is assumed to be $\Delta\Re = \Re/3$, as in (Nayakshin and Wilkinson 2013).

3.4.2 Differences between §3 Nayakshin and Wilkinson (2013) and our model (§4.2)

The differences between both models are the following:

1. In their model, the satellite galaxies were formed by a dark matter halo with baryonic matter and a disc gas. In this project, the galaxies are also formed by a stellar disc and stellar bulge. While they calculated the fraction of the mass retained for the dwarf galaxies, this work is carried out for masses $1.0 \times 10^{10} \leq M_{200}^{\rm sat}/M_{\odot} \leq 1.1 \times 10^{12}$
2. Their ram pressure is caused by a host halo with Milky Way-size. In this thesis masses from group to rich cluster are employed.
3. They used a Hubble constant of $H_0 = 100.0$ km s^{-1} Mpc^{-1}, whereas in this work the constant is taken from (Planck Collaboration et al. 2016). In addition, they did not use Eq. (5)-(7) from (Muñoz-Cuartas et al. 2011) in order to obtain the concentration parameter of the halo.
4. The projection cosine to study the ram pressure for different angles is included. In addition, the shock front travels at a constant velocity such as $V_{\rm sh} = 1000,\ 1500,\ 2000$ km s^{-1} rather than $V_{\rm sh} = 300,\ 500,\ 1000$ km s^{-1}.
5. While they studied the process of stripping for the local universe, this project aims to study it from low to high redshift.

3.4.3 Testing against previous works

Firstly, §4.1.1 focuses on the gravitational restoring force per unit of area. The procedure is as follows:

1. Criterion to set the height.
2. A comparison with Gunn and Gott (1972) work in order to demonstrate that by making a more sophisticated and realistic satellite galaxy, the force will be more powerful.
3. Analysis at different redshifts.

The most up-to-date ΛCDM cosmological parameters from measurement of the Planck satellite (Planck Collaboration et al. 2016) are used in § 4.1.1 and §4.2. The assumptions have been deemed in order to reproduce a Milky Way galaxy are the following:

- Virial mass of the halo, thin and thick disc and stellar bulge according to (Bland-Hawthorn and Gerhard 2016).
- Thin disc is assumed to be the stellar disc and the thin is considered the gas one.
- While at low redshift the fraction of stellar mass to gas disc mass $f_{\rm d}$ is roughly $\sim 5-10\%$, the discs are usually gas rich with a $f_{\rm d} \sim 0.5$ the disc mass at high redshift. In order to satisfy this fact, Equation 33 is adjusted to

$$f_{\rm d} = 0.1\ (1+z)^{1.5} \tag{39}$$

- The bulge is assumed to be the oldest component of the galaxy, then it can keep bulge mass constant at all redshifts. The bulge-stellar mass fraction is consider $f_{\rm bulge} = 0.30$. However, this hypothesis is very stringent and clearly not realistic. For a given cluster and satellite galaxy, the values used are the following:

		Parameters	Value
Satellite galaxy	**Dark matter halo**	$M_{200}^{\rm sat}\ (M_\odot)$	1.10×10^{12}
		$f_{\rm h}$	0.09
	Stellar and gas disc	f_*	0.03
		$R_{*,\rm d}$ (kpc)	0.05 $R_{200}^{\rm sat}$
		$z_{*,\rm d}$ (kpc)	0.06 $R_{*,\rm d}$
	Bulge	$f_{\rm bulge}$	0.30
		$R_{\rm b}$ (kpc)	0.05 $R_{*,\rm d}$
Ram pressure	**Galaxy cluster**	$M_{200}^{\rm host}\ (M_\odot)$	$3 \times\ 10^{14}$
	Other	$f_{\rm sh}$	0.05
		Ψ°	0
		$V_{\rm sh}$ (km s^{-1})	1000
Other		z	0, 1, 2
		H_0 (km s^{-1} Mpc^{-1})	68.70

Table 1: Values used in §4.1.1 and §4.2.

Secondly, we want to check if the model proposed in this project is valid and applicable to larger ram pressures. To do this, their values in §3, are used in order to reproduce their results, omitting the stellar disc and the stellar bulge. They considered three dwarf galaxies were subjected to the stripping effect by a host galaxy with Milky Way-size. They depicted the fraction of retained mass those galaxies after interaction with shock as a function of the distance between the host-satellite $\Re$.

		Parameters	Value
Satellite galaxy	**Dark matter halo**	$M_{200}^{\rm sat}$ $(M_\odot)$	7.85×10^8, 6.29×10^9, 5.03×10^{10}
		$f_{\rm h}$	0.1
		$c^{\rm sat}$	10
	Gas disc	$f_{\rm d}$	0.05
		$R_{\rm d}$ (kpc)	0.05 $R_{200}^{\rm sat}$
		$z_{\rm d}$ (kpc)	0.06 $R_{\rm d}$
Ram pressure	**Host galaxy**	$M_{200}^{\rm host}$ $(M_\odot)$	2×10^{12}
		$c^{\rm host}$	20
	Other	$f_{\rm sh}$	0.05
		Ψ°	0
		$V_{\rm sh}$ (km s^{-1})	500
Other		z	0
		H_0 (km s^{-1} Mpc^{-1})	100

Table 2: Values used in §4.1.2.

3.4.4 Cluster-size AGN shock

Thirdly, in §4.2 it is made a detailed analysis of $\delta_{\rm ret_{d,h}}(< \Re)$ dependence with respect to

1. **Redshift $\mathbf{z = 0, 1, 2}$**: $\Psi = 0^\circ$, $V_{\rm sh} = 1000$ km s^{-1}, $M_{200}^{\rm host} = 3 \times 10^{14}\ M_\odot$.
   (a) $M_{200}^{\rm sat} = 1.1 \times 10^{12}\ M_\odot$
   (b) $1.0 \times 10^{10} \leq M_{200}^{\rm sat}/M_\odot \leq 1.1 \times 10^{12}$
2. **Shocked shell outflow velocity $\mathbf{V_{sh} = 1000}$, 1500, 2000** km s^{-1}: $z = 2$, $\Psi = 0$, $M_{200}^{\rm host} = 3 \times 10^{14}\ M_\odot$.
   (a) $M_{200}^{\rm sat} = 1.1 \times 10^{12}\ M_\odot$
   (b) $1.0 \times 10^{10} \leq M_{200}^{\rm sat}/M_\odot \leq 1.1 \times 10^{12}$
3. **Inclined angle $\mathbf{\Psi = 0^\circ, 30^\circ, 60^\circ}$**: $V_{\rm sh} = 1000$ km s^{-1}, $z = 2$, $M_{200}^{\rm host} = 3 \times 10^{14}\ M_\odot$.
   (a) $M_{200}^{\rm sat} = 1.1 \times 10^{12}\ M_\odot$
   (b) $1.0 \times 10^{10} \leq M_{200}^{\rm sat}/M_\odot \leq 1.1 \times 10^{12}$
4. **Cluster mass 'group' with $M_{200}^{\rm host} = 5 \times 10^{13}\ M_\odot$, a 'cluster' with $3 \times 10^{14}\ M_\odot$ and finally a 'rich cluster'** with $2 \times 10^{15}\ M_\odot$: $\Psi = 0^\circ$, $V_{\rm sh} = 2 \times 10^3$ km s^{-1}, $z = 2$.
   (a) $M_{200}^{\rm sat} = 1.1 \times 10^{12}\ M_\odot$
   (b) $1.0 \times 10^{10} \leq M_{200}^{\rm sat}/M_\odot \leq 1.1 \times 10^{12}$

4 Results

4.1 Testing against previous works

4.1.1 Gravitational restoring force

As it is mentioned in §2 and §3.1, the gravitational acceleration from the satellite galaxy depends on the radius and height. Ideally, it would be preferable to set the height at which this function is maximum along ζ-direction for any radii, so it is guaranteed the gas in the galaxy will be more difficult to be stripped. Then, the distance at which this occurs is now explored. Looking at gradient of the potential formulæ, some terms decrease in inverse proportion (Equations 27, 38) and other exponentially (Eq. 35) in relation with the projected radius R, so it is a fact that the stronger this gradient the closer to the centre of the disc (gas disc case) and halo (gas halo case). Also worth noting is the discontinuity exactly at $R = 0$, which the acceleration tends to infinity. For that reason that a non-zero projected radius has must deemed.

Figure 6(a) shows all contributors in the gravitational acceleration for a given radius (a non-zero projected radius closed to the disc centre is chosen, called $R_{\rm min}$) as a function of the height ζ. The bulge (yellow solid curve) is dominant and just relevant closed to the disc plane. The major contributor at far distances is the dark matter halo's (blue dashed curve). Moreover, the stellar and gas disc (red and magenta solid curves, respectively), which follow a hyperbolic tangent profile (see Equation 35), saturates practically at short height due to the small scale heights $\zeta_{*,\rm d}$. In addition, adding all terms, the total acceleration is maximum along the ζ-direction for height closed to the disc plane at minimum projected radius case. Furthermore, the dependence of the gravitational acceleration as a function of the projected radius at the mentioned height, denominated ζ_{min} can be viewed in Figure 6(b). It is possible to verify the bulge is influential for small radii whereas the stellar disc is the major term until distances near to the virial radius, where the dark matter and gas halo dominate. It must be emphasized that the amplitude of each component are influenced by their respectively mass, scale length and height.

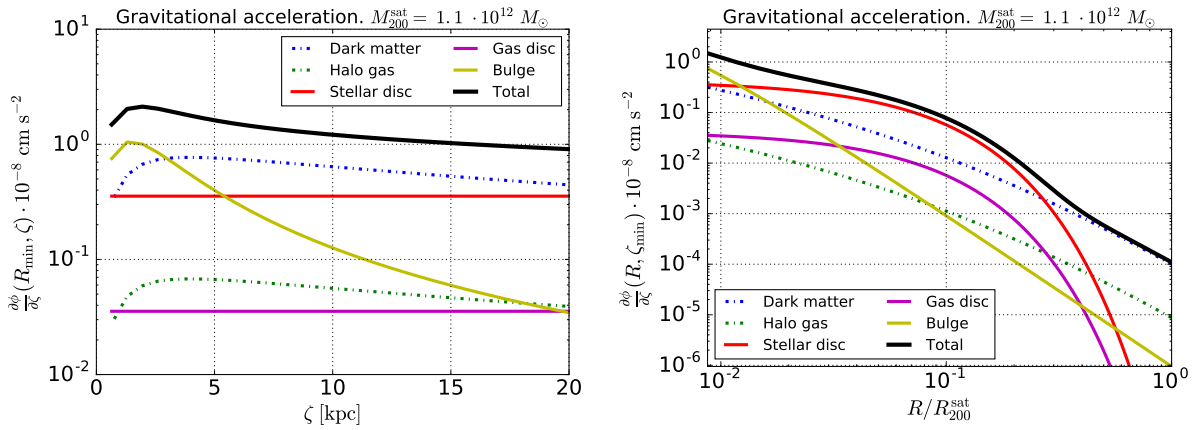

(a) As a function of height ζ at a minimum radius.

(b) As a function of radius normalized to the virial one at a minimum height.

Figure 6: Gravitational acceleration from Milky Way-size galaxy at local Universe. All contributors have been considered: dark matter halo (blue dashed curve), halo gas (green dashed curve), stellar disc (red solid line/curve), gas disc (magenta solid line/curve), bulge (yellow solid curve/line) and total (dark solid curve).

As for the gravitational restoring force from the satellite galaxy for the disc case, Roediger and Hensler (2005) suggested the possibility to choose either the maximal restoring force per unit

of area inside the disc or the maximal at any height (see their Figure 8). The above mentioned authors showed that both choices are quite similar, differing at lower ram pressure (see their Figure 9). In order to investigate what height should be considered, the mentioned force per unit of area as a function ζ for a set radius $R_{\rm set}$ is plotted using our parameters taken from Table 1. One can check in Figure 7 that both possibilities submitted by the cited paper. The criterion of this project is to use this maximum force at all times, so the height ζ will be set when this happens.

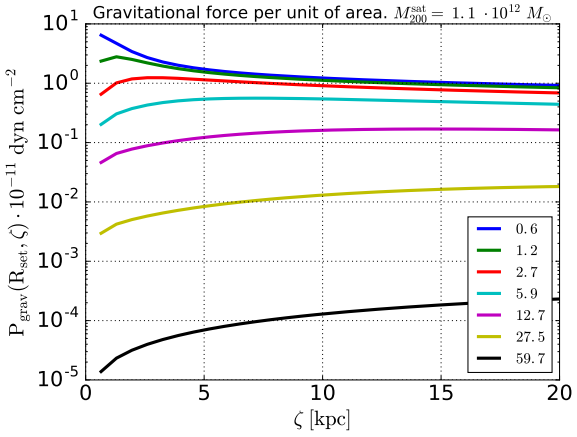

Figure 7: Gravitational restoring force per unit of area from Milky Way-size galaxy as a function of the height ζ at a given radius and local Universe. The legend shows different $R_{\rm set}$ values in kpc.

Three different gravitational accelerations are now compared in Figure 8(a): the black solid curve corresponds to the Gunn and Gott (1972) case which is superposed to the yellow dashed curve, the stellar disc potential gradient, as one would expect[9]. The remaining color curves are lightly greater because all contributors have been taken into account. It should be mentioned that the height at which the gradients are maximum have taken. In addition, as one sees, the difference between both cases is not significant. Firstly, when one looks at small heights, the difference between accelerations is greater because the bulge dominates in that range. For larger radius, the disc dominates and the contribution of the bulge is practically negligible, hence it looks similar to Gunn&Gott. Secondly, when one observes towards higher heights and small radii, the difference between both cases is lower since the bulge hardly contributes. At higher radii, the halo is the largest contributor. Therefore, the gravitational pressure $P_{\rm grav}$ in this model resists much longer to the shock front than Gunn and Gott (1972) case (see Figure 8(b)).

[9]In respect of the stellar disc potential gradient, the function begins to be constant from heights very close to the plane of the disc and remains constant at all times, so that is why one does not appreciate more dashed curves. However, the maximum of the function varies as a function of the height for a given radius.

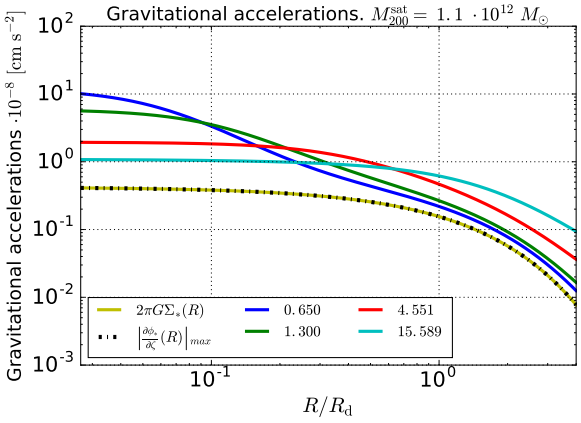

(a) Gravitational accelerations: Gunn-Gott (yellow solid curve), stellar gradient (black dashed curve) and total gradient (solid lines at different colours).

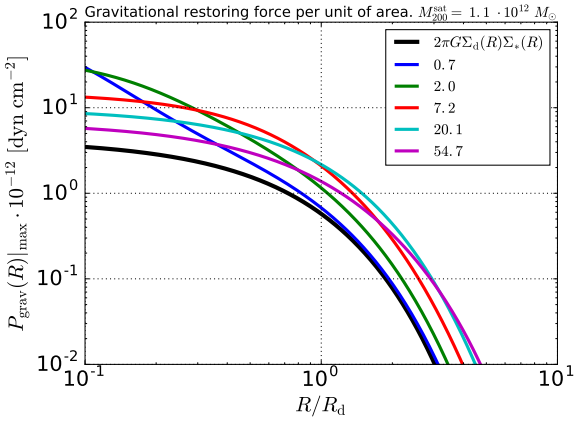

(b) Gravitational restoring force per unit of area: Gunn-Gott (black solid curve), total gradient (solid curves at different colours).

Figure 8: Both curves are a function of the projected radius over the scale length of the disc R/R_d. Milky Way-size galaxy case. The number of the legend shows the height ζ values at which the function ($\frac{\partial\phi}{\partial\zeta}(R)$ for the former case and $\Sigma_{\rm gas}(R)\frac{\partial\phi}{\partial z}(R)$ for the latter one) is maximum (in kpc).

Finally, the gravitational restoring force per unit of area are plotted at different redshifts in Figure 9. There is a notable difference between both cases, around an order of magnitude, so it is confirmed that at large z the galaxies will retain more of their gas. This fact is due originated by several factors: the higher the redshift, the greater the critical density of the universe and the hubble parameter. In addition, the radius of the virial will be smaller and the haloes will be more concentrated. Furthermore, the fraction of the stellar disc to the gas disc $f_{\rm d}$ is up to 50% at high z, against $5-10\%$ percent at the local universe.

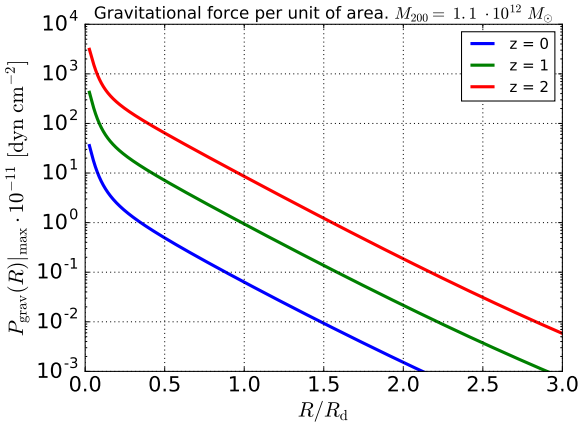

Figure 9: Gravitational restoring force per unit of area from Milky Way-size galaxy as a function of the radius over the scale length R/R_d at a given height. From low to high redshifts. The function is set to be at which is maximum at height $\zeta \sim 0.5$ *kpc*.

4.1.2 (Nayakshin and Wilkinson 2013)'s work

The overcomes seen in the §3 (Nayakshin and Wilkinson 2013), that is, $\delta_{\rm ret_{d,h}}$ are now reproduced. In that section, they studied the stripping process whose host halo is a Milky Way-size and satellite galaxies with virial velocities $V_{200}^{\rm sat}$ such as $15, 30, 60$ km s^{-1}. They analyzed the RP effect for different shocked shell outflow velocities, $V_{\rm sh}$ such as $300, 500, 1000$ km s^{-1} which are constant at all times. In order to simplify the results, only the intermediate velocity is taken into account. The stellar bulge and disc are disregarded in terms of the gravitational restoring force. In addition, the ram pressures encountered by satellite are exactly the same (NFW shell shock case).

Figure 10(a) and 10(b) illustate the mass retained fraction in percentage for the disc and halo, respectively. The gas in the least massive satellite galaxy, whose virial velocity is 15 km s^{-1}, is stripped more efficiently because their gravitational restoring force is lower respect to other. While the gas in the halo is practically stripped before reaching the virial radius of the host galaxy, the gas in the disc is preserved at closer galactocentric distances, because the disc is more compact and its gravitational force is greater than the halo.

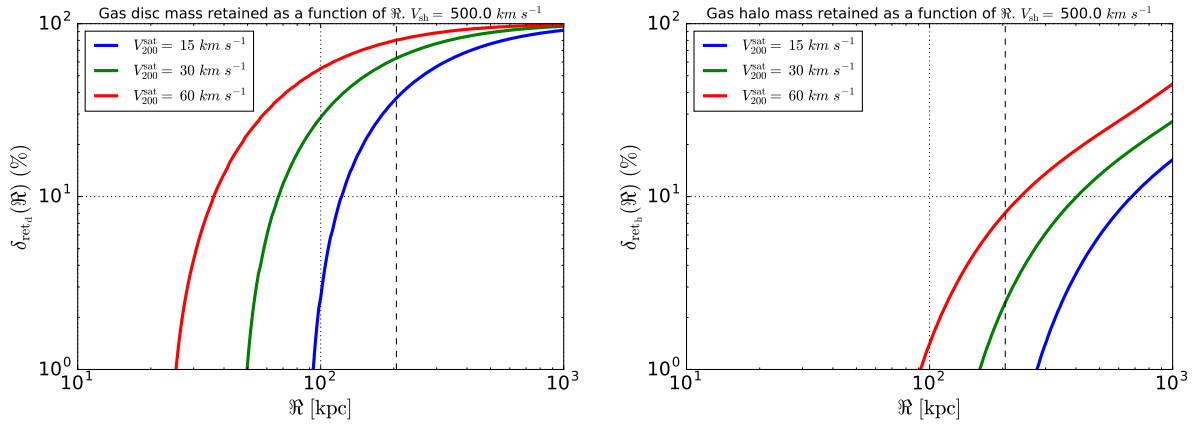

(a) Gas disc component.

(b) Halo gas component.

Figure 10: Retained mass fraction after shock passage as a function of the galactocentric radius ℜ. (Nayakshin and Wilkinson 2013) values has been used in our model (Table 2). Vertical dashed line is located at host's virial radius.

To gauge the effectiveness of the model presented in this project, Table 3 shows a comparison between our results and those obtained by Nayakshin and Wilkinson (2013) denoted as (N&W12). For instance, by examining the red curve of the left panel, corresponding to the disc component with virial velocity $V_{200}^{\rm sat} = 60$ km s^{-1}, it is possible to observe that it loses half of its gas at 85 kpc in relation with the galactocentric radius, while it completely loses its gas around 25 kpc. As one can see in Table 3, the fractions of gas retained from the disc are practically identical in both the (N&W12) model and ours. However, this fact does not occur in the case of halo. The difference is quite remarkable, decreasing as the percentages are smaller and at higher velocities. One possible reason for this phenomena could be the calculation of its respective stripping radius. More specifically, the gas halo surface density may have been calculated differently and erroneously. Although, the calculations differ in this case, physics is obeyed: the more massive the halo, the greater the gravitational force is and, therefore, retains its gas for a longer time. In addition, the gas in the halo is not going to play an important role in the study of the stripping effect because it hardly resists the shock force, losing all its gas at distances close to host galaxy virial radius.

$V_{200}^{\rm sat}$ (km s^{-1})	Gas component	$\delta_{\rm ret}$ (%)	$\Re_{\rm N\&W12}$ (kpc)	$\Re$ (kpc)	ϵ_a (kpc)
15	**Disc**	50	250	250	0
		0	90	90	0
	Halo	50	1000	>1000	-
		0	170	270	100
30	**Disc**	50	150	150	0
		0	50	50	0
	Halo	50	750	>1000	>250
		0	90	160	70
60	**Disc**	50	85	85	0
		0	25	25	0
	Halo	50	400	>1000	>600
		0	50	90	60

Table 3: Comparison between overcomes obtained by our calculations and N&W12 model. The distance $\Re$ at which the retained mass by the satellite galaxy after the shock passage for the disc and halo component $\delta_{\rm ret}$ is a 50% and 0% respect to the total one is shown here. The difference between both models in $\Re$ is shown as the absolute error $\epsilon_{\rm a}$. It must be noted that they are estimated data.

In conclusion, the model perfectly describes the overcomes presented by N&W12 for the case of the disc, while in the case of the halo the behavior is analogous, although the calculations are different. Then, physics is considered valid and it is feasible to affirm that our model is consistent and applicable at higher scales.

4.2 Cluster-size AGN shock

In this section, an in-depth study of the stripping process is made, calculating the percentage of gas mass retained for different events, such as redshift, velocity shock, inclination angle and host halo masses. The satellite galaxies masses have a range between 10^{10} $M_\odot$ and 10^{12} $M_\odot$ (Milky Way-size). One expects that the physical phenomena that were obtained previously also occur at large scales, that is, the more massive the galaxy is, the more gas it will retain both for the halo case and for the disc. On the contrary to previous section, the stellar bulge, stellar disc and gas halo are now deemed as contributors to the gravitational restoring force.

It is now supposes the interaction between winds coming from a supermassive black hole located in the center of a cluster with the intracluster medium. This shock will spread throughout the galaxy cluster expelling the gas from a satellite galaxy as massive as the Milky

Way. Let us assume a shock velocity with $V_{\rm sh} = 1000$ km s^{-1}, an inclination angle equal to zero degrees $\Psi = 0°$ (maximum effect of ram pressure), galaxy cluster with mass $M_{200}^{\rm host} = 3 \cdot 10^{14}\ M_{\odot}$. In order to see the effect on the galaxy, the fraction of the gas retained is represented as a function of the clustercentric radius $\Re$ in Figure 10. In the same image, it is possible to appreciate the results obtained both for gas in the disc (solid curves) and in the halo (dashed curves) at different redshift (the red color corresponds to $z = 0$, blue to $z = 1$ and green to $z = 2$). The Figure 11 confirms that the higher the redshift is, the harder to be stripped for disc component as well as gas halo component. That is due to several reasons: in reference to the halo, the greater the z, the greater the hubble parameter, the critical density of the universe, the more concentrated the halo (the value of c is lower because the virial radius of is smaller). Consequently, the virial velocity is faster and, in addition to the surface density, resulting a stronger gravitational restoring force.

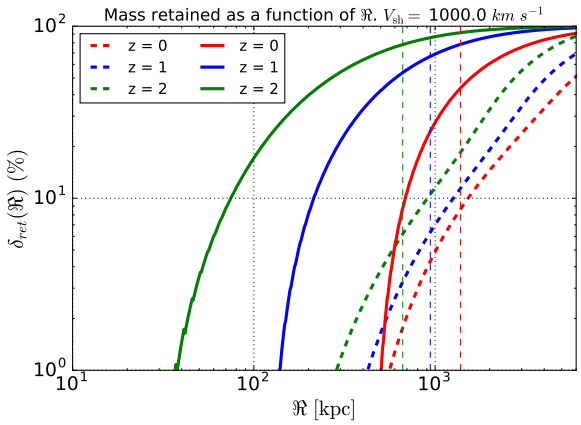

Figure 11: Gas disc mass (solid curves) and gas halo mass (dashed curves) retained as a function of the clustercentric distance $\Re$. Vertical green, blue and red dashed lines are located at cluster's virial radius for redshift $z = 0, 1, 2$ respectively. The study is carried out for different redshifts and set to be $M_{200}^{\rm host} = 3.0 \cdot 10^{14}\ M_{\odot}$, $M_{200}^{\rm sat} = 1.1 \cdot 10^{12}\ M_{\odot}$, $V_{\rm sh} = 1000$ km s^{-1} and $\Psi = 0°$.

The component of the halo is not interesting to study since it loses practically all its gas before reaching the virial radius of the cluster, so the project is only focused on the component of the disc. Now, this phenomenon is explored by satellite galaxies up to two orders of magnitude smaller than Milky Way. As representative examples in Figure 12, 3D surface graph $\delta_{\rm ret_d}$ is plotted as a function of the satellite virial mass and the distance $\Re$ from low redshift ($z = 0$) to high one ($z = 2$)[10]. Looking at low redshift in Figure 12(a), 19(a), one finds that physics is analogous to the case of dwarf galaxies see in §4.1.2. Both images demonstrate that the more heavy the galaxy is, the harder to be stripped for disc component. The red solid curve seen in Figure 11, corresponds to the curve located at the side of the 3D surface for the most massive satellite galaxy. Comparing the overcomes from low redshift (Figure 12(a), 19(a)) to high redshift (Figure 12(b), 19(b)), there is a fairly wide separation between the distances at which $\delta_{\rm ret} = 50\%$: 1500 kpc, 600 kpc and 250 kpc for redshift 0, 1 and 2, respectively. This can be understood since the gravitational pressure between each z is one order of magnitude (it can be seen in Figure 9, mentioned before). Then, it is proved that as the z is larger, also the gravitational force is also, so the galaxy conserves the gas for a longer time: so that $P_{\rm grav_{z=2}} > P_{\rm grav_{z=1}} > P_{\rm grav_{z=0}}$.

[10]To appreciate the effect in more details, the reader can also analyse both figures from different perspective in the Appendix A.2.

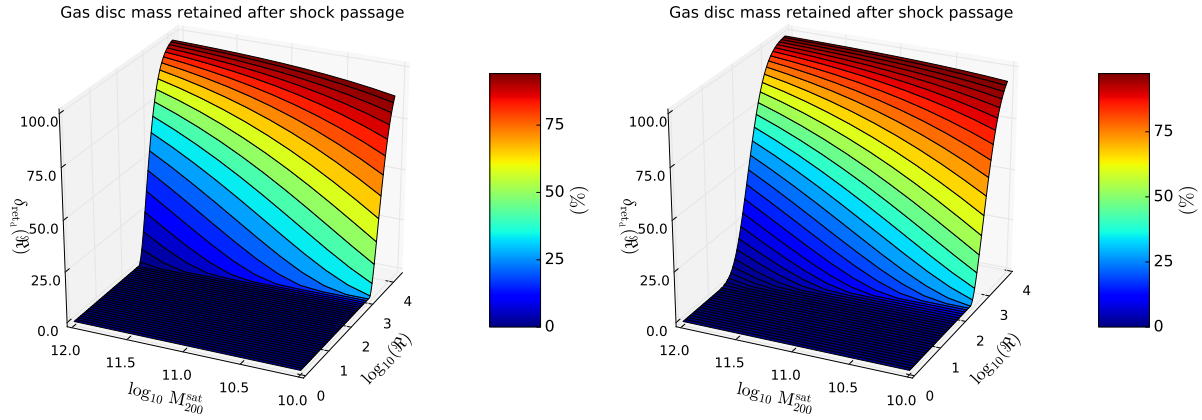

(a) $z = 0$. (b) $z = 2$.

Figure 12: Gas disc mass retained as a function of the satellite virial masses and the clustercentric distance $\Re$. The study is carried out for different redshifts and set to be $M_{200}^{\rm host} = 3 \cdot 10^{14}\ M_\odot$, $V_{\rm sh} = 10^3$ km s^{-1}, $\Psi = 0°$. To see the effect in more details, the reader can also analyse both figures from a different perspective in Figure 19.

The effect that ram pressure would have into faster shock velocities is now analysed. First, one focuses on a satellite galaxy (Milky Way-size), a cluster, at zero inclination angle and high redshift. The fact that the velocity of the shock is greater, leads to the gas being lost more easily, so that $P_{\rm sh_{2000\ km\ s^{-1}}} > P_{\rm sh_{1500\ km\ s^{-1}}} > P_{\rm sh_{1000\ km\ s^{-1}}}$ (it can be also seen in Figure 23). Half of the mass of the gas in the disk is expelled to the same distance for both cases, in particular, to 500 kpc, so that a change in the velocity of the shock practically does not affect the satellite galaxy yet. The gas will have been expelled completely at distances roughly to 100 kpc when the shock velocity are 1500 km s^{-1} and 2000 km s^{-1}, while $V_{\rm sh} = 1000$ km s^{-1} the galaxy is less susceptible to the shock front, retaining gas up to $\Re \sim 25$ kpc. While the difference between $P_{\rm grav}$ for $z = 1$ and $z = 2$ is one order of magnitude, it also occurs for the cases of $P_{\rm sh_{1000\ km\ s^{-1}}}$ and $P_{\rm sh_{2000\ km\ s^{-1}}}$. Therefore, one can observe a a difference of an approximately 100 kpc of the gas lost for both cases (see Table 4).

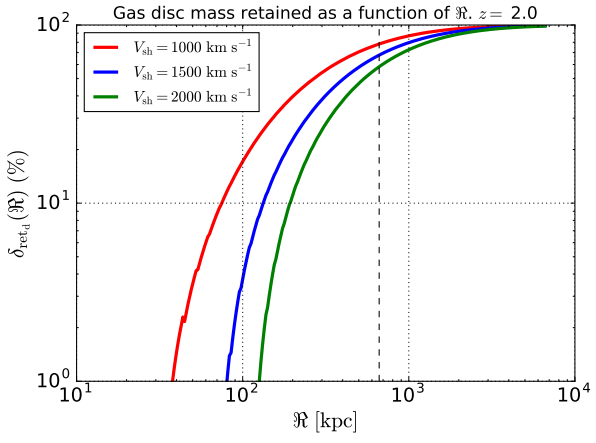

Figure 13: Gas disc mass retained as a function of the clustercentric distance $\Re$. Black vertical dashed line is located at cluster's virial radius. The study is carried out for different shock velocities and set to be $M_{200}^{\rm sat} = 1.1 \cdot 10^{12}\ M_\odot$, $M_{200}^{\rm host} = 3 \cdot 10^{14}\ M_\odot$, $\Psi = 0°$, $z = 2$.

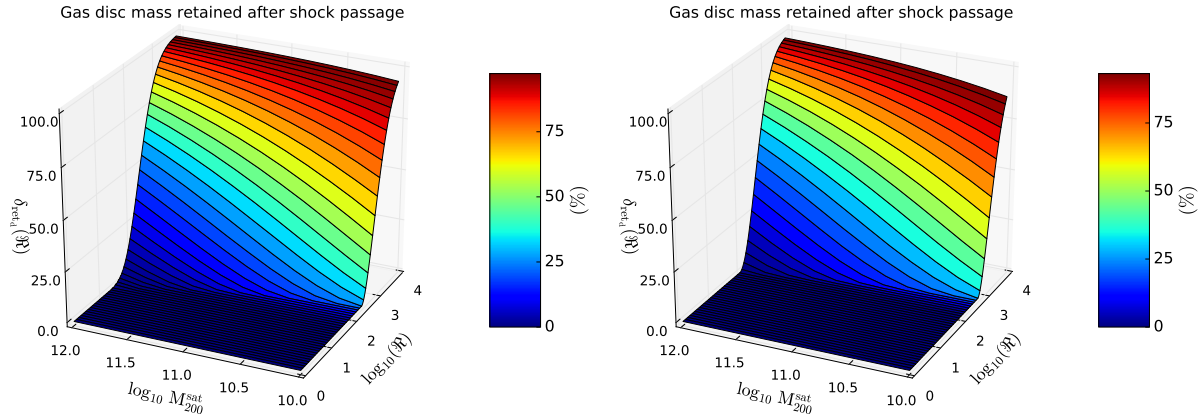

(a) $V_{\rm sh} = 1 \cdot 10^3$ km s^{-1}. (b) $V_{\rm sh} = 2 \cdot 10^3$ km s^{-1}.

Figure 14: Gas disc mass retained as a function of the satellite virial masses and the clustercentric distance $\Re$. The study is carried out for different shock velocities and set to be $M_{200}^{\rm host} = 3{\cdot}10^{14}\ M_\odot$, $\Psi = 0°$, $z = 2$. To see the effect in more details, the reader can also analyse both figures from a different perspective in Figure 20.

On the other hand, the inclination angle is now varied from $\Psi = 0°$ to $30°$ and $\Psi = 60°$ for a given shock velocity, redshift and virial mass in Figure 15. As the angle of inclination is greater, the cosine is taking increasingly smaller values, causing the ram pressure to be weaker, so that $\mathrm{P_{sh}}_{\Psi=0°} > \mathrm{P_{sh}}_{\Psi=30°} > \mathrm{P_{sh}}_{\Psi=60°}$. This is the parameter that the least affects the satellite galaxy which travels "seamlessly" through the ICM until tens of kpc from the host's center. The difference between the gas retained for the case of 0 and 30 degrees is practically negligible. When the angle reaches 60 degrees, the separation is somewhat larger in relation to low degrees, where the pressure may be a few tenths higher in Figure 23. Accordingly, the galaxy will be less damaged at high degrees, reaching to contain small percentages of gas at fairly short distances. Performing the same process for different satellite galaxies (see Figure 16), the same effect is found. The more massive the galaxy is the more gas it will retain for a longer time, as in all cases previously analysed.

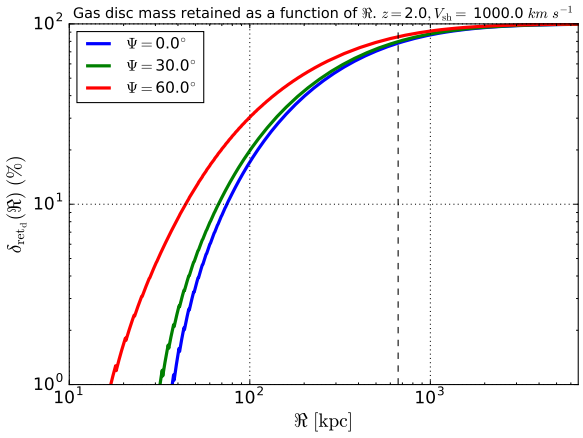

Figure 15: Gas disc mass retained as a function of the clustercentric distance $\Re$. Black vertical dashed line is located at cluster's virial radius. The study is carried out for different inclination angles and set to be $M_{200}^{\rm sat} = 1.1 \cdot 10^{12}\ M_\odot$, $M_{200}^{\rm host} = 3 \cdot 10^{14}\ M_\odot$, $V_{\rm sh} = 1 \cdot 10^3$ km s^{-1}, $z = 2$.

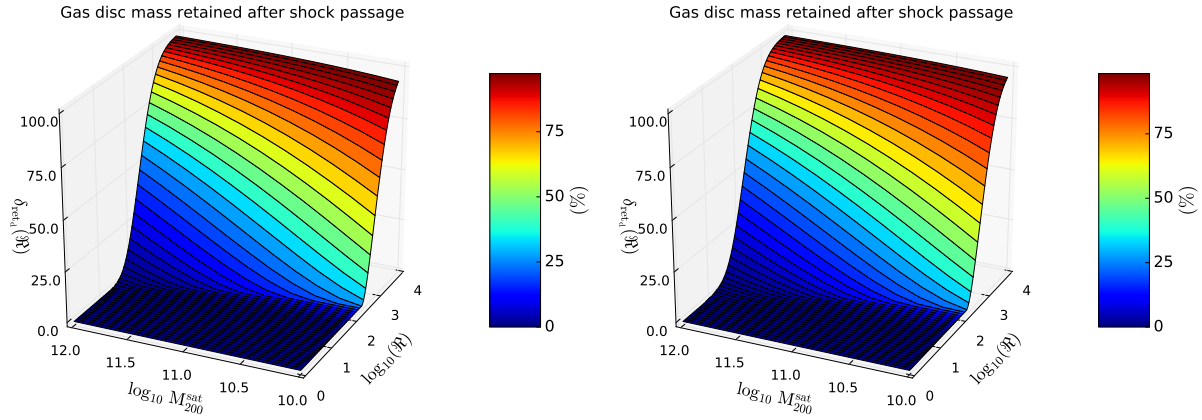

(a) $\Psi = 0°$. (b) $\Psi = 60°$.

Figure 16: Gas disc mass retained as a function of the satellite virial masses and the clustercentric distance $\Re$. The study is carried out for different inclination angles and set to be $M_{200}^{\rm host} = 3 \cdot 10^{14}\ M_\odot$, $V_{\rm sh} = 1 \cdot 10^3$ km s^{-1}, $z = 2$. To see the effect in more details, the reader can also analyse both figures from a different perspective in Figure 21.

Finally, the dependence on the mass of the host galaxy is now studied from galaxy groups $10^{13}\ M_\odot$ to rich clusters $10^{15}\ M_\odot$. To do this, the stripping process is explored at high redshift $z = 2$, setting the inclination angle to zero $\Psi = 0°$ and the velocity of the shell at $V_{\rm sh} = 1000$ km s^{-1}. Differences were founded in the mass of the shell being expelled from the host $M_{\rm sh}(< \Re)$, being a function of the clustercentric radius. As the mass of the halo is proportional to the density of the shell and it grows as it travels through the ICM, it is more powerful at positions that are increasingly distant from the center of the cluster. When the halo mass is of a rich cluster type have a major impact on the galaxy (green solid curve in Figure 17). Moreover, the stronger the ram pressure stripping is, the less massive galaxies are (see Figure Figure 18), as in previously studied cases.

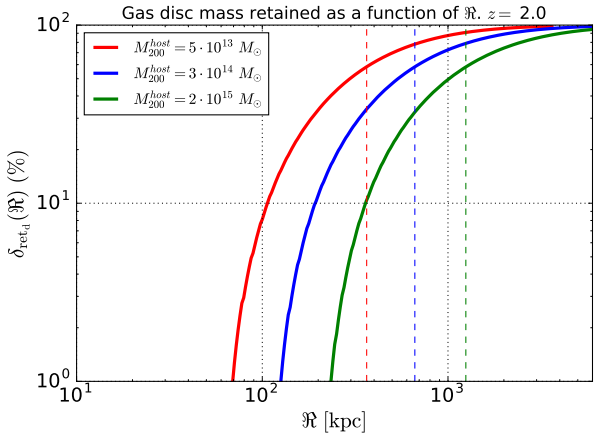

Figure 17: Gas disc mass retained as a function of the clustercentric distance $\Re$. Vertical red, blue and green dashed lines are located at cluster's virial radius for group/cluster masses $M_{200}^{\rm host} = 5 \cdot 10^{13}\ M_\odot, M_{200}^{\rm host} = 3 \cdot 10^{14}\ M_\odot, M_{200}^{\rm host} = 2 \cdot 10^{15}\ M_\odot$ respectively. The study is carried out for different inclination angles and set to be $M_{200}^{\rm sat} = 1.1 \cdot 10^{12}\ M_\odot$, $V_{\rm sh} = 1 \cdot 10^3$ km s^{-1}, $\Psi = 0°$, $z = 2$.

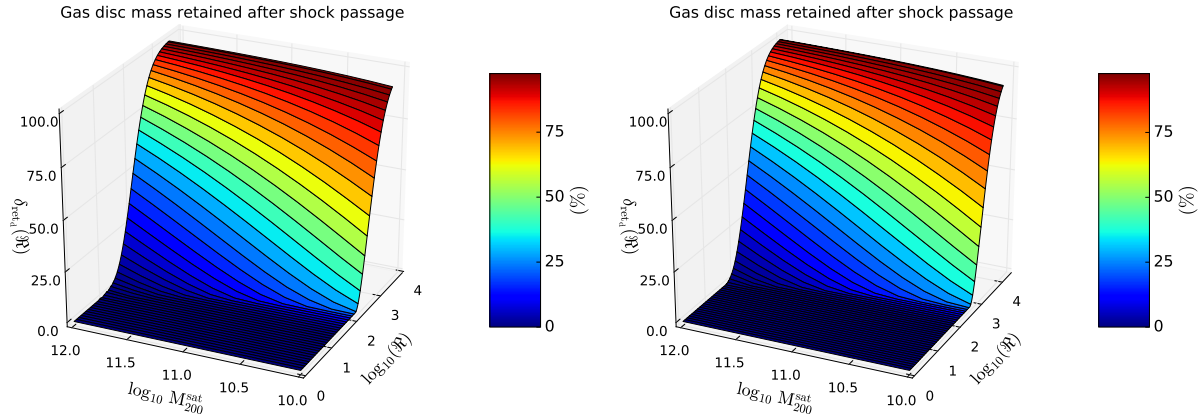

(a) $M_{200}^{\rm host} = 5 \cdot 10^{13}\ M_{\odot}$. (b) $M_{200}^{\rm host} = 2 \cdot 10^{15}\ M_{\odot}$.

Figure 18: Gas disc mass retained as a function of the satellite virial masses and the clustercentric distance $\Re$. The study is carried out for different group/cluster galaxy masses and set to be $V_{\rm sh} = 1 \cdot 10^3$ km s^{-1}, $\Psi = 0°$, $z = 2$. To see the effect in more details, the reader can also analyse both figures from a different perspective in Figure 22.

It should be noted that all the cases studied in this section are collected in Table 4.

5 Conclusions

The major effect of ram-pressure stripping is that of the ICM. We looked at an additional effect coming from powerful AGN outflows and shock. This project starts showing in §4.1.1 that while the bulge is dominant and just relevant closed to the disc plane, the stellar disc is the major contributor to the gravitational force for radii where the bulge ceases to dominate at heights close to that plane. In addition, the dark matter halo component is the greatest for radii close to the virial and longer heights. The study demonstrates that, if all contributors are considered, the gravitatonial forces overcomes the suggested by Gunn and Gott (1972). Therefore, the greater the redshift is the greater the gravitational restoring force is.

To gauge the effectiveness of the model, results from (Nayakshin and Wilkinson 2013) were reproduced in §4.1.2. The outcomes are identical to their paper for the disc component, while it differs for the halo, although is not interesting to study because the gas is practically stripped before reaching the virial radius of the host galaxy. Thus, this work has proven to be perfectly valid and applicable at large scales. It was demonstrated in §4.2 that since the disc is more concentrated than the halo, it retains more gas because its gravitational force is higher.

In addition, we map $\delta_{\mathrm{ret_d}}$ as a function of $\Re$ and M_{200}^{sat}. We demonstrate that the more massive the satellite galaxy is, the harder to be stripped for all cases. We find that the disc component a spiral galaxy with Milky-Way size can lose all its gas if it is within 500, 140 and 35 kpc of the centre of the host galaxy at redshift $z = 0$, $z = 1$ and $z = 2$, respectively. Thus, when the redshift is higher, the gas will be retained for a longer time. We have also confirmed that the less massive the halo host and the slower the velocity of the shell, the lower the effect of the ram pressure on the satellite galaxies. Furthermore, when the angle of inclination is lower, the pressure exerted by the shock will tend to be maximum, as well as its impact on the galaxy. Of all the cases studied, the most effective ram pressure will be when the V_{sh} reaches 2000 km s^{-1}, while the weakest is when the inclination angle is set to be 60 degrees.

The project could be **more realistic** if the following points had been considered:

1. The overdensity of haloes as a function of the redshift.
2. In a more realistic model, the shock shell velocity decreases as a function of the cluster-centric radius.
3. A major shortcoming of the model is considering real values of scale length and height for Milky Way's stellar and gas dics such as in (Bland-Hawthorn and Gerhard 2016): $R_* = 2.6$ kpc, $z_* = 300$ pc, $R_{\mathrm{d}} = 2.0$ kpc, $z_{\mathrm{d}} = 900$ pc. The problem lies on the fact that the stellar disc component would dominates the gravitational acceleration for any height. However, this fact would not be correct, hence the model was adjusted with the parameters given in Tables 1 and 2. Gravitational terms should then be reviewed in depth.

In order to know if the total kinetic energy from the outflow of the NFW shell shock model is similar to the energy emitted by a supermassive black hole at its maximum activity, Eq. 3 may be compared to Eq. 9. As an example, if one assumes a supermassive black hole with mass $10^9 M_\odot$ that emits during a time much shorter than the typical dynamic time of a cluster $t_{\mathrm{BH}} \sim 10^5$ yr < 1 Gyr, one obtained an energy lower than the total kinetic energy E_{sh} for any case studied. In addition, if (King 2003)'s formula is used rather than Eq. 3, it obtains results closest to the NFW shell shock method, . As a conclusion, the fraction f_{sh} could have been overestimated because the values V_{sh} are typical in those environments.

It could conduct a research study to fully understand how outflows and shocks through the intra-cluster medium (ICM) reduce the star formation rate and change the colour of galaxies. Another thing to check in the future is the relative contribution of shocks to the ram-pressure stripping produced by the ICM. Probably, most of the gas has already been removed by this effect before the galaxy reaches distances from the cluster center small enough that shocks have appreciable effect.

On the other hand, if the host halo is assumed to be an isothermal sphere[11] the ICM density Eq. 43 can be determined through hydrostatic equilibrium. Then, this density profile can be used. Furthermore, another possibility to describe the density of the ICM is β-model (Eq. 48), model that agrees with the observations and is commonly used (Cavaliere and Fusco-Femiano 1976).

Finally, these calculations can be verified by comparing our analytical models with hydrodynamical cosmological simulations such as EAGLE (Evolution and Assembly of GaLaxies and their Environments) and Cluster-EAGLE, which investigate the formation and evolution of galaxies.

[11] It is not realistic because the cluster's temperature decreases as a function of the radius (not close to its center).

References

Abadi, M. G., B. Moore, and R. G. Bower (1999). "Ram pressure stripping of spiral galaxies in clusters". In: *Monthly Notices of the Royal Astronomical Society* 308, pp. 947–954. DOI: 10.1046/j.1365-8711.1999.02715.x. eprint: astro-ph/9903436.

Benson, A. J. (2010). "Galaxy formation theory". In: *Physics Reports* 495.2, pp. 33–86. ISSN: 0370-1573. DOI: https://doi.org/10.1016/j.physrep.2010.06.001. URL: http://www.sciencedirect.com/science/article/pii/S037015731000150X.

Bezanson, R. et al. (2009). "The Relation Between Compact, Quiescent High-redshift Galaxies and Massive Nearby Elliptical Galaxies: Evidence for Hierarchical, Inside-Out Growth". In: 697, pp. 1290–1298. DOI: 10.1088/0004-637X/697/2/1290. arXiv: 0903.2044 [astro-ph.CO].

Bland-Hawthorn, J. and O. Gerhard (2016). "The Galaxy in Context: Structural, Kinematic, and Integrated Properties". In: 54, pp. 529–596. DOI: 10.1146/annurev-astro-081915-023441. arXiv: 1602.07702.

Boettcher, M., D. E. Harris, and H. Krawczynski (2012). "Relativistic Jets from Active Galactic Nuclei". In: WILEY-VCH, pp. 374–382. ISBN: 9783527410378. DOI: 10.1002/9783527641741.

Bryan, G. L. and M. L. Norman (1998). "Statistical Properties of X-Ray Clusters: Analytic and Numerical Comparisons". In: 495, pp. 80–99. DOI: 10.1086/305262. eprint: astro-ph/9710107.

Cattaneo, A. et al. (2009). "The role of black holes in galaxy formation and evolution". In: *Nature* 460, pp. 213–219. DOI: 10.1038/nature08135.

Cavaliere, A. and R. Fusco-Femiano (1976). "X-rays from hot plasma in clusters of galaxies". In: 49, pp. 137–144.

collaboration, ESO/GASP (2017a). *Name: JO204, Constellation: Sextans*. URL: https://www.eso.org/public/images/eso1725a/. (accessed: 22.01.2018).

— (2017b). *Name: JW100, Constellation: Pegasus*. URL: https://www.eso.org/public/images/eso1725b/. (accessed: 22.01.2018).

— (2017c). *Name: JW206, Constellation: Aquarius*. URL: https://www.eso.org/public/images/eso1725d/. (accessed: 22.01.2018).

Dekel, A. and J. Silk (1986). "The origin of dwarf galaxies, cold dark matter, and biased galaxy formation". In: 303, pp. 39–55. DOI: 10.1086/164050.

Diaferio, A. et al. (2001). "The spatial and kinematic distributions of cluster galaxies in a ΩCDM universe: comparison with observations". In: *Monthly Notices of the Royal Astronomical Society* 323.4, pp. 999–1015. DOI: 10.1046/j.1365-8711.2001.04303.x. eprint: /oup/backfile/content_public/journal/mnras/323/4/10.1046/j.1365-8711.2001.04303.x/2/323-4-999.pdf. URL: http://dx.doi.org/10.1046/j.1365-8711.2001.04303.x.

Domainko, W. et al. (2004). "Feedback from intra-cluster supernovae on the ICM in cooling flow galaxy clusters". In: *A&A* 425.2, pp. L21–L24. DOI: 10.1051/0004-6361:20040178. URL: https://doi.org/10.1051/0004-6361:20040178.

Dutton, A. A. et al. (2011). "On the evolution of the velocity-mass-size relations of disc-dominated galaxies over the past 10 billion years". In: 410, pp. 1660–1676. DOI: 10.1111/j.1365-2966.2010.17555.x. arXiv: 1006.3558.

Fabian, A.C. (2012). "Observational Evidence of Active Galactic Nuclei Feedback". In: *Annual Review of Astronomy and Astrophysics* 50.1, pp. 455–489. DOI: 10.1146/annurev-astro-081811-125521. eprint: https://doi.org/10.1146/annurev-astro-081811-125521. URL: https://doi.org/10.1146/annurev-astro-081811-125521.

Forman, W. et al. (2007). "Filaments, Bubbles, and Weak Shocks in the Gaseous Atmosphere of M87". In: 665, pp. 1057–1066. DOI: 10.1086/519480. eprint: astro-ph/0604583.

Geach, James E. et al. (2011). "On the Evolution of the Molecular Gas Fraction of Star-Forming Galaxies". In: *The Astrophysical Journal Letters* 730.2, p. L19. URL: http://stacks.iop.org/2041-8205/730/i=2/a=L19.

Gómez−Fernández, J.L. and W. Steffen (2009). "Agujeros negros supermasivos". In: *Investigación y Ciencia* 396, pp. 30–40.

Gunn, J. E. and III Gott J. R. (1972). "On the Infall of Matter Into Clusters of Galaxies and Some Effects on Their Evolution". In: 176, p. 1. DOI: 10.1086/151605.

Hernquist, L. (1993). "Structure of merger remnants. II - Progenitors with rotating bulges". In: 409, pp. 548–562. DOI: 10.1086/172686.

King, A. (2003). "Black Holes, Galaxy Formation, and the MBH-σ Relation". In: *The Astrophysical Journal Letters* 596.1, pp. L27–L29. URL: http://stacks.iop.org/1538-4357/596/i=1/a=L27.

Kino, M. et al. (2009). "High energy emission from AGN cocoons in clusters of galaxies". In: *Astronomische Nachrichten* 330.2-3, pp. 257–260. DOI: 10.1002/asna.200811170. "arXiv": 0901.2968.

Langer, N. (2012). "Presupernova Evolution of Massive Single and Binary Stars". In: 50, pp. 107–164. DOI: 10.1146/annurev-astro-081811-125534. arXiv: 1206.5443 [astro-ph.SR].

Marcolini, A., F. Brighenti, and A. D'Ercole (2003). "Three−dimensional simulations of the interstellar medium in dwarf galaxies I. Ram pressure stripping". In: *Monthly Notices of the Royal Astronomical Society* 345.4, pp. 1329–1339. DOI: 10.1046/j.1365-2966.2003.07054.x. eprint: https://onlinelibrary.wiley.com/doi/pdf/10.1046/j.1365-2966.2003.07054.x. URL: https://onlinelibrary.wiley.com/doi/abs/10.1046/j.1365-2966.2003.07054.x.

Mayer, L. et al. (2006). "Simultaneous ram pressure and tidal stripping; how dwarf spheroidals lost their gas". In: 369, pp. 1021–1038. DOI: 10.1111/j.1365-2966.2006.10403.x. eprint: astro-ph/0504277.

McNamara, B. R. et al. (2009). "An Energetic AGN Outburst Powered by a Rapidly Spinning Supermassive Black Hole or an Accreting Ultramassive Black Hole". In: 698, pp. 594–605. DOI: 10.1088/0004-637X/698/1/594. arXiv: 0811.3020.

Mo, H. J., S. Mao, and S. D. M. White (1998). "The formation of galactic discs". In: *Monthly Notices of the Royal Astronomical Society* 295, pp. 319–336. DOI: 10.1046/j.1365-8711.1998.01227.x. eprint: astro-ph/9707093.

Muñoz-Cuartas, J. C. et al. (2011). "The redshift evolution of Λ cold dark matter halo parameters: concentration, spin and shape". In: *Monthly Notices of the Royal Astronomical Society* 411.1, pp. 584–594. DOI: 10.1111/j.1365-2966.2010.17704.x. eprint: /oup/backfile/content_public/journal/mnras/411/1/10.1111/j.1365-2966.2010.17704.x/2/mnras0411-0584.pdf. URL: http://dx.doi.org/10.1111/j.1365-2966.2010.17704.x.

Murakami, I. and A. Babul (1999). "Interaction between the intergalactic medium and galactic outflows from dwarf galaxies". In: *Monthly Notices of the Royal Astronomical Society* 309, pp. 161–179. DOI: 10.1046/j.1365-8711.1999.02810.x. eprint: astro-ph/9906084.

Navarro, J. F., C. S. Frenk, and S. D. M. White (1997). "A Universal Density Profile from Hierarchical Clustering". In: 490, pp. 493–508. DOI: 10.1086/304888. eprint: astro-ph/9611107.

Nayakshin, S. and M. I. Wilkinson (2013). "A link between feedback outflows and satellite galaxy suppression". In: *Monthly Notices of the Royal Astronomical Society* 433.1, pp. 324–331. DOI: 10.1093/mnras/stt724. eprint: /oup/backfile/content_public/journal/mnras/433/1/10.1093_mnras_stt724/1/stt724.pdf. URL: http://dx.doi.org/10.1093/mnras/stt724.

Patterson, R. J. and T. X. Thuan (1992). "UGC 7636 and NGC 4472 - Tidal interaction between a stripped dwarf irregular and a giant elliptical galaxy". In: 400, pp. L55–L58. DOI: 10.1086/186648.

Planck Collaboration et al. (2016). "Planck 2015 results. XIII. Cosmological parameters". In: 594, A13, A13. DOI: 10.1051/0004-6361/201525830.

Poggianti, B. M. et al. (2016). "Jellyfish galaxy candidates at low redshift". In: *The Astronomical Journal* 151.3, pp. 78–98. DOI: 10.3847/0004-6256/151/3/78.

Robertson, H. P. (1935). "Kinematics and World-Structure". In: 82, p. 284. DOI: 10.1086/143681.

— (1936a). "Kinematics and World-Structure II." In: 83, p. 187. DOI: 10.1086/143716.

— (1936b). "Kinematics and World-Structure III." In: 83, p. 257. DOI: 10.1086/143726.

Roediger, E. and M. Brüggen (2006). "Ram pressure stripping of disc galaxies: the role of the inclination angle". In: 369, pp. 567–580. DOI: 10.1111/j.1365-2966.2006.10335.x. eprint: astro-ph/0512365.

— (2007). "Ram pressure stripping of disc galaxies orbiting in clusters - I. Mass and radius of the remaining gas disc". In: 380, pp. 1399–1408. DOI: 10.1111/j.1365-2966.2007.12241.x. arXiv: 0707.2698.

Roediger, E. and G. Hensler (2005). "Ram pressure stripping of disk galaxies. From high to low density environments". In: 433, pp. 875–895. DOI: 10.1051/0004-6361:20042131.

Trujillo, I. et al. (2007). "Strong size evolution of the most massive galaxies since z $\sim$ 2". In: 382, pp. 109–120. DOI: 10.1111/j.1365-2966.2007.12388.x. arXiv: 0709.0621.

van Dokkum, P. G. et al. (2010). "The Growth of Massive Galaxies Since z = 2". In: 709, pp. 1018–1041. DOI: 10.1088/0004-637X/709/2/1018. arXiv: 0912.0514.

von der Linden, A. et al. (2010). "Star formation and AGN activity in SDSS cluster galaxies". In: *Monthly Notices of the Royal Astronomical Society* 404, pp. 1231–1246. DOI: 10.1111/j.1365-2966.2010.16375.x. arXiv: 0909.3522.

Walker, A. G. (1935). "On Riemanntan Spaces with spherical symmetry about a line, and the conditions for isotropy in GENJ Relativity". In: *The Quarterly Journal of Mathematics* os-6.1, pp. 81–93. DOI: 10.1093/qmath/os-6.1.81. eprint: /oup/backfile/content_public/journal/qjmath/os-6/1/10.1093/qmath/os-6.1.81/2/os-6-1-81.pdf. URL: http://dx.doi.org/10.1093/qmath/os-6.1.81.

Wang, H. H et al. (2010). "Equilibrium initialization and stability of three-dimensional gas discs". In: *Monthly Notices of the Royal Astronomical Society* 407.2, pp. 705–720. DOI: 10.1111/j.1365-2966.2010.16942.x. eprint: /oup/backfile/content_public/journal/mnras/407/2/10.1111/j.1365-2966.2010.16942.x/2/mnras0407-0705.pdf. URL: http://dx.doi.org/10.1111/j.1365-2966.2010.16942.x.

A Appendix

A.1 Gas intracluster medium density profiles

The pressure of the hot halo gas in the intracumular medium may be determined assuming **hydrostatic equilibrium** of a stable, gravitationally bound system, ICM.

$$F_{\rm g}(r) = F_{\rm p}(r) \quad \rightarrow \quad \rho_{\rm g}(r)\frac{d\phi_{\rm g}(r)}{dr} = \rho_{\rm g}\frac{GM_{\rm grav}(<r)}{r^2} = -\frac{dP_{\rm g}(r)}{dr} \tag{40}$$

where $M_{\rm grav}(<r)$ is the gravitational mass of the cluster, $\rho_{\rm g}(r)$ the gas density and $P_{\rm g}(r)$ the gas pressure. It also may be interpreted as momentum conservation for a fluid with internal friction[12] where momentum of the fluid is equal to the gravitational compression. For a system in equilibrium

$$\cancelto{0}{\frac{\partial\vec{v}(r)}{\partial t} + (\vec{v}(r)\cdot\nabla)\,\vec{v}(r)} = -\frac{\nabla P_{\rm g}(r)}{\rho_{\rm g}(r)} + \vec{g}(r) \qquad \rightarrow \qquad \frac{\nabla P_{\rm g}(r)}{\rho_{\rm g}(r)} = -\nabla\phi(r) \tag{41}$$

solving the previous formula for density of the gas and assuming an **isothermal sphere** for the dark matter halo[13]

$$\frac{d\phi(r)}{dr} = -\frac{1}{\rho_{\rm g}(r)}\frac{dP_{\rm g}(r)}{dr} = -\frac{1}{\rho_{\rm g}(r)}\frac{d}{dr}\left(\rho_{\rm g}(r)\frac{k_{\rm B}T_{\rm g}}{\langle m\rangle}\right) = -\left(\frac{k_{\rm B}T_{\rm g}}{\langle m\rangle}\right)\frac{d\ln\rho_{\rm g}(r)}{dr} \tag{42}$$

The **gas density of the halo** is determined by integrating the previous equation

$$\begin{aligned}\rho_{\rm g}(r) &= \rho_{\rm g_0}\exp\left[-\left(\frac{\langle m\rangle}{k_{\rm B}T_{\rm g}}\right)\phi(r)\right] = \rho_{\rm g_0}\exp\left[\left(\frac{\langle m\rangle}{k_{\rm B}T_{\rm g}}\right)\left(\frac{4\pi G\delta_{\rm c}\rho_{\rm crit}r_{\rm s}^3}{r}\right)\ln\left(1+\frac{r}{r_{\rm s}}\right)\right] = \\ &= \rho_{\rm g_0}\exp\left[\eta\frac{r_{\rm s}}{r}\ln\left(1+\frac{r}{r_{\rm s}}\right)\right] = \rho_{\rm g_0}\left(1+r/r_{\rm s}\right)^{\eta\frac{r_{\rm s}}{r}}\end{aligned} \tag{43}$$

with $\rho_{\rm g_0}$ is the gas density at the cluster's center and $\eta = \left(\frac{4\pi G\delta_{\rm c}\rho_{\rm crit}\langle m\rangle r_{\rm s}^2}{k_{\rm B}T_{\rm g}}\right)$. In order to obtain the density at the center, the relation between $M_{200,gas}$ and $M_{200,\rm DM}$ is considered

$$M_{200,\rm g} = f_{\rm b}M_{200} \qquad M_{200,\rm DM} = f_{\rm DM}M_{200} \tag{44}$$

where $f_{\rm b} = \Omega_{\rm b}/\Omega_{\rm m}$ and $f_{\rm DM} = (\Omega_{\rm m}-\Omega_{\rm b})/\Omega_{\rm m}$ are the fraction of the baryon mass and the dark matter mass respect to the total mass of the cluster, respectively. If both terms are divided

$$\frac{M_{200,\rm g}}{M_{200,\rm DM}} = \frac{\Omega_{\rm b}}{(\Omega_{\rm m}-\Omega_{\rm b})} \tag{45}$$

Baryon mass in the halo $M_{200,g}$ is given by

$$M_{200,\rm g} = 4\pi\int_0^{r_{200}} dr\; r^2\rho_{\rm g}(r) = 4\pi\rho_{\rm g_0}\int_0^{r_{200}} dr\; r^2\left(1+r/r_{\rm s}\right)^{\eta\frac{r_{\rm s}}{r}} \tag{46}$$

[12] Viscosity.

[13] The gas pressure follows the ideal gas law: $P_{\rm g}(r) = (\gamma-1)\rho_{\rm g}u$, where $u = \frac{1}{\gamma-1}\frac{k_{\rm B}T_{\rm g}}{\langle m\rangle}$, γ is the heat capacity ratio, $k_{\rm B}$ the Boltzmann's constant, $T_{\rm g}$ the temperature of the cluster hot gas, the mean mass of the particle $\langle m\rangle = \mu m_H$, m_H hydrogen mass and μ mean molecular weight.

Finally, the gas density at the cluster's center is calculated by inserting Eq. 45 here

$$\rho_{\mathrm{g}_0} = \frac{M_{200,\mathrm{g}}}{4\pi \int_0^{r_{200}} dr\ r^2\,(1 + r/r_\mathrm{s})^{\eta\,\frac{r_\mathrm{s}}{r}}} \tag{47}$$

The gas density distribution is also given by the **hydrostatic isothermal β model**, which is based on the aproximate King model for galaxies in clusters (Cavaliere and Fusco-Femiano 1976). This model has been employed in analyses of X-ray emitting hot gas in clusters of galaxies. The density profile β-model is given by

$$\rho_{g_\beta}(r) = \rho_{g_{\beta_0}} \left[1 + \left(\frac{r}{r_c}\right)^2\right]^{-\frac{3}{2}\beta} \tag{48}$$

where r_c is the core radius of the gas distribution which is commonly considered a fraction of scale radius r_s and β a free parameter.

A.2 Cluster-size AGN shock

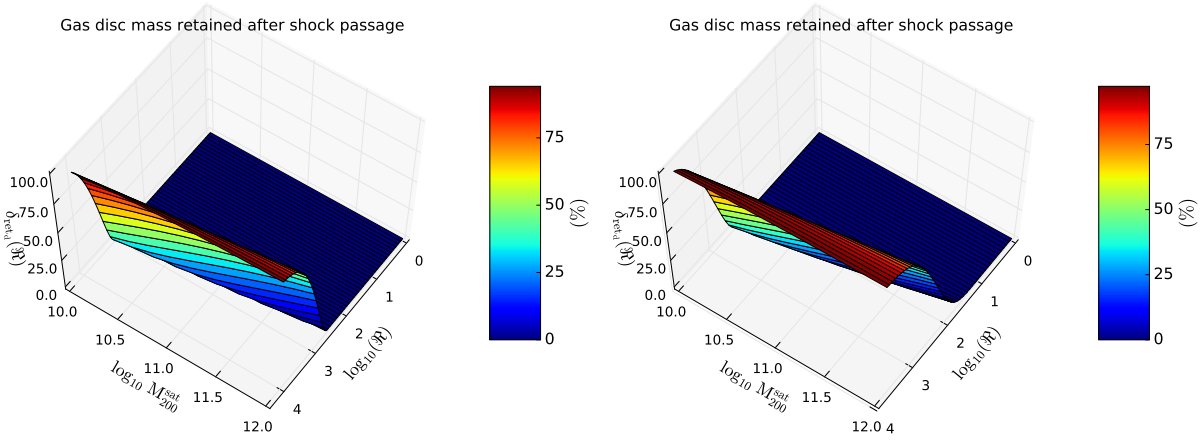

(a) $z = 0$. (b) $z = 2$.

Figure 19: Gas disc mass retained as a function of the satellite virial masses and the clustercentric distance $\Re$. The study is carried out for different redshifts and are set to be $M_{200}^{\rm cluster} = 3 \cdot 10^{14}\ M_\odot$, $V_{\rm sh} = 10^3$ km s^{-1}, $\Psi = 0°$. Analogous to Figure 12.

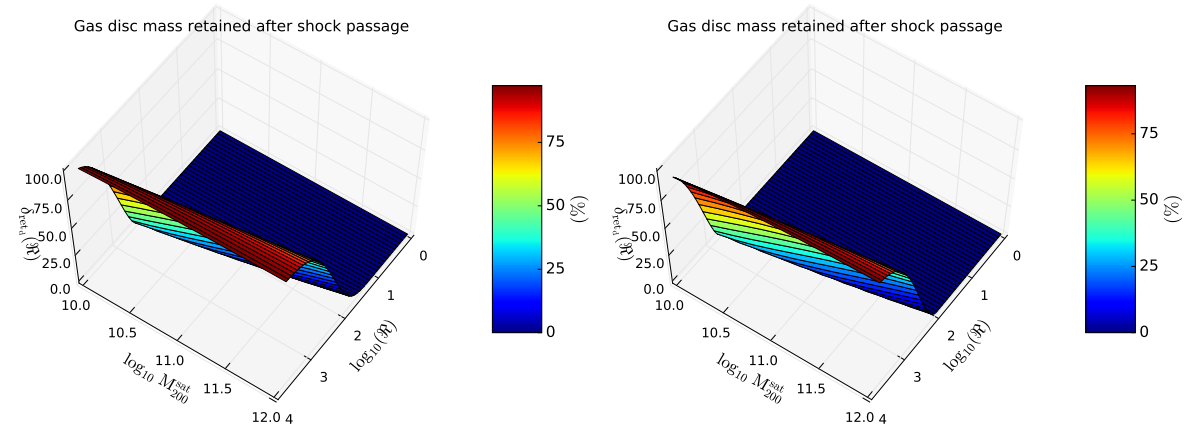

(a) $V_{\rm sh} = 1 \cdot 10^3$ km s^{-1}. (b) $V_{\rm sh} = 2 \cdot 10^3$ km s^{-1}.

Figure 20: Gas disc mass retained as a function of the satellite virial masses and the clustercentric distance $\Re$. The study is carried out for different shock velocities and set to be $M_{200}^{\rm cluster} = 3 \cdot 10^{14}\ M_\odot$, $\Psi = 0°$, $z = 2$. Analogous to Figure 14.

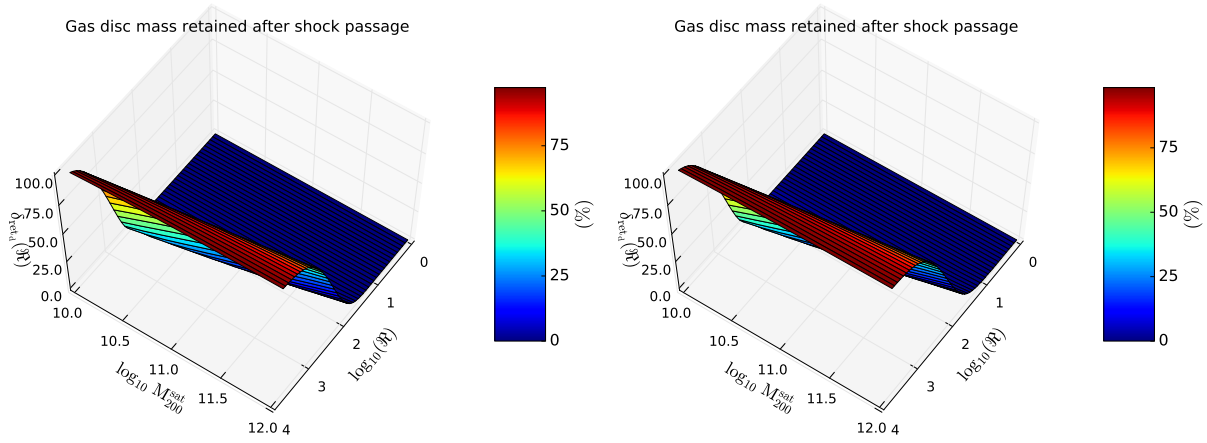

(a) $\Psi = 0°$. (b) $\Psi = 60°$.

Figure 21: Gas disc mass retained as a function of the satellite virial masses and the clustercentric distance $\Re$. The study is carried out for different inclination angles and set to be $M_{200}^{\rm cluster} = 3 \cdot 10^{14}\ M_\odot$, $V_{\rm sh} = 1 \cdot 10^3$ km s^{-1}, $z = 2$. Analogous to Figure 16.

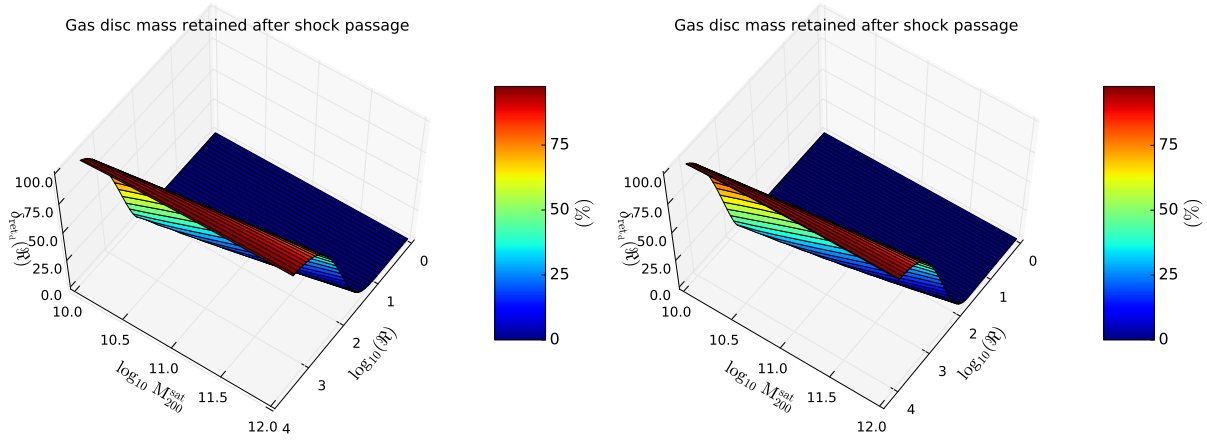

(a) $M_{200}^{\rm cluster} = 5 \cdot 10^{13}\ M_\odot$. (b) $M_{200}^{\rm cluster} = 2 \cdot 10^{15}\ M_\odot$.

Figure 22: Gas disc mass retained as a function of the satellite virial masses and the clustercentric distance $\Re$. The study is carried out for different group/cluster galaxy masses and set to be $V_{\rm sh} = 1 \cdot 10^3$ km s^{-1}, $\Psi = 0°$, $z = 2$. Analogous to Figure 18.

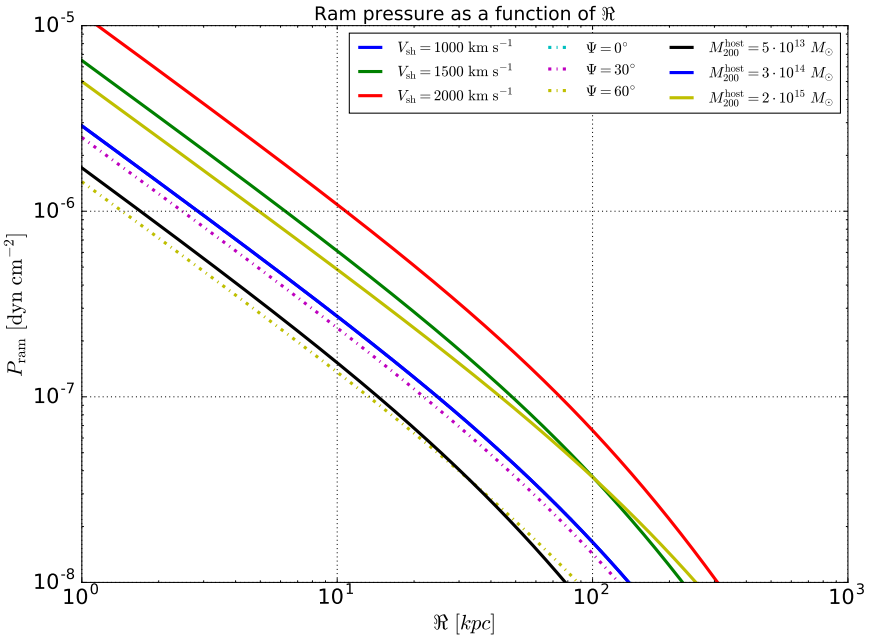

Figure 23: Ram pressure as a function of ℜ. All cases are collected here at high redshift.

Parameters	**Values**	δ_{ret} (%)	ℜ (kpc)
z	**0**	50	1500
		0	500
	1	50	600
		0	140
	2	50	250
		0	35
V_{sh} (km s^{-1})	**1000**	50	500
		0	25
	1500	50	500
		0	80
	2000	50	600
		0	120
Ψ (°)	**0**	50	270
		0	35
	30	50	250
		0	30
	60	50	200
		0	15
M_{200}^{host} ($M_\odot$)	**$5 \cdot 10^{13}$**	50	300
		0	70
	$3 \cdot 10^{14}$	50	550
		0	115
	$2 \cdot 10^{15}$	50	1000
		0	230

Table 4: Results obtained from all the cases studied in § 4.2. It must be noted that the values are estimated data.